ROSAT OBSERVATIONS OF THE PLEIADES CLUSTER.
I. X-RAY CHARACTERISTICS OF A COEVAL STELLAR POPULATION

G. Micela and S. Sciortino

Istituto ed Osservatorio Astronomico di Palermo
Palazzo dei Normanni, 90134 Palermo, Italy
E-mail: gmicela@oapa.astropa.unipa.it, ssciortino@oapa.astropa.unipa.it

V. Kashyap

Department of Astronomy & Astrophysics, The University of Chicago
5640 South Ellis Avenue, Chicago, IL 60637
E-mail: kashyap@oddjob.uchicago.edu

F.R. Harnden, Jr.

Harvard-Smithsonian Center for Astrophysics
60 Garden Street, Cambridge, MA 02138
E-mail: frh@cfa.harvard.edu

R. Rosner

Department of Astronomy & Astrophysics and Enrico Fermi Institute
The University of Chicago, 5640 South Ellis Avenue, Chicago, IL 60637
E-mail: rrosner@oddjob.uchicago.edu

Received 1994 June 13 ; Revised ...

ABSTRACT

We report the results of a deep X-ray survey of the core region of the Pleiades cluster carried out with the ROSAT Observatory. In a single PSPC field ($\sim 1^\circ$ radius), we detect 99 of 214 Pleiades member stars, and compute upper limits for the remainder. We have detected all early dM stars which fell within 20 arcmin of the field center, where the instrument sensitivity is highest. We have computed maximum-likelihood integral X-ray luminosity functions in various $B-V$ intervals, and have compared the results with previous studies of Pleiades cluster. Our results support the contention that B and dA star 'detections' are likely due to X-ray emission from lower-mass companions; we confirm the existence of a stellar-age vs. X-ray–luminosity relation found with *Einstein* for dG stars, and extend it to dK and dM stars; and we construct an essentially statistically complete X-ray luminosity function for Pleiades dG stars and an almost complete X-ray luminosity function for dK stars. We have verified the stellar-rotation vs. X-ray–luminosity relation for Pleiades dG stars, and show that a similar relation does not hold for dK stars. Indeed, it appears that some stellar parameters other than age and/or rotation rate must affect the level of X-ray emission of Pleiades dG and dK stars. We demonstrate the lack of measurable variability in X-ray emission at small time scales of $\sim$ 6 months (except for flares), and the presence of variability by a factor two on timescales of $\sim$ 10 yr in at least 15% of Pleiades members. The magnitude of this variability (by $\sim$ a factor two) is too small to account for the spread of the X-ray luminosity functions.

Subject headings: open cluster and associations: individual (Pleiades) - stars: late-type - stars: rotation - surveys - X-Rays: stars

1. INTRODUCTION

Studies of open stellar clusters have long been used as a standard tool for disentangling evolutionary effects. Because stellar activity depends crucially on stellar rotation, which in turn displays a strong secular dependence (see review by Rosner, Golub, & Vaiana 1985), such open clusters have also proven to be crucial to distinguishing between truly evolutionary effects on stellar activity and effects which are due primarily to the rotation rate itself (cf. Stern et al. 1981; Walter 1983; Caillault & Helfand 1985; Micela et al. 1985; Micela et al. 1988; Micela et al. 1990, hereafter Paper I; Schmitt et al. 1990). Recently new ROSAT data have allowed us to study the coronal emission and its relation with stellar rotation rate as well as with other stellar parameters in various nearby open clusters, namely: the Hyades (Stern et al. 1992, 1994; Pye et al. 1994), the Pleiades (Schmitt et al. 1993, Stauffer et al. 1994, Hodgkin, Jameson & Steele 1995), Praesepe (Randich & Schmitt 1994), and IC 2391 (Patten & Simon 1993).

In the case of the classic Pleiades cluster, there have been several extensive X-ray studies based on *Einstein* Observatory data (Caillault & Helfand 1985; Micela et al. 1985; Paper I), primarily from the Imaging Proportional Counter (IPC; Gorenstein, Harnden & Fabricant 1981) observations. The most extensive compilation of *Einstein* data (Paper I) reports a total of 85 Pleiades member stars as X-ray sources, and upper bounds on X-ray emission for a further 198 member stars.

Recently, two other surveys of the Pleiades Cluster in the X-ray regime have been carried out using ROSAT observations: The first is based on data collected during the ROSAT All-Sky Survey (RASS) (Schmitt et al. 1993), and the second is derived from a set of 3 pointed exposures (Stauffer et al. 1994) to the north of the field described here. The first survey, carried out at a lower sensitivity than the *Einstein* IPC survey, detected 28 X-ray emitting Pleiades, including 3 that were not detected before, while in the latter survey a total of 317 X-ray sources (at 2.5 σ confidence level) were reported, of which 171 could be identified with certain or probable Pleiades members.

The ROSAT observations discussed in this paper were motivated by three considerations: First, to probe the stellar luminosity function for young stars below the mean X-ray luminosity for the field stars; second, to determine whether significant variations existed in stellar X-ray properties as a function of spectral type for young stars, especially at the low-mass end of the main sequence, and at the edge of the boundary for surface convection zones on the Zero Age Main Sequence (ZAMS); and third, to study the X-ray spectral properties of these young stars, asking in particular whether these highly active and young stars are distinguishable from their older (but still active) field star counterparts. The results presented in this paper in large part resolve the first issue, while the second issue is still left open by available data. The third issue (requiring detailed X-ray spectral analysis) will be the subject of a forthcoming paper.

Our paper is organized as follows: §2 describes the selection procedures for compiling our optical catalog of Pleiades cluster members; §3 presents the X-ray data and describes our data analysis method; §4 presents the X-ray luminosity functions and discusses their relevance to X-ray activity levels with emphasis on the low-mass stars; §5 discusses the variability in X-ray emission exhibited by Pleiades stars. In §6 we discuss the relation between rotation and stellar activity for low-mass stars, and estimate the magnetic fields confining the hot plasma in 'saturated' stellar coronae; and in §7 we summarize the conclusions. We provide further description of our data selection procedure and count determination methods in Appendix A.

2. THE OPTICAL CATALOG

The nucleus of the composite optical catalog used in the present study is the catalog compiled from published literature for the *Einstein* investigations of the Pleiades Cluster in Paper I. We have extended this compilation to include results published in the last few years and have added those stars from recent Pleiades optical surveys (Stauffer et al. 1991; Rosvick, Mermilliod, & Major 1992) with membership probabilities greater than 0.2 (our acceptance threshold chosen for the *Einstein* compilation). Our revised reference catalog includes a total of 664 Pleiades stars, with a large increase in the number of the faintest members, and extends the completeness limit to $V \sim 18$, at least in the region near Alcyone observed with ROSAT. This completeness limit corresponds to $M_V \sim 12.5$, i.e., to middle-M stars at the cluster distance (d = 127 pc).

To minimize field star contamination in our catalog, stars listed by Stauffer et al. (1991) without quoted membership probability have not been included. However we have retained them in the process of matching optical objects with otherwise unidentified X-ray sources, and consider these counterparts as possible cluster members.

We have adopted a similar approach for the Hambly, Hawkins, & Jameson (1993, HHJ) catalog where the contamination with field stars is severe, even exceeding 50% for $m_I \sim 18.5$. Hence we consider these possible faint cluster members separately from other stars, and discuss them in the section (§4.6) devoted to the X-ray emission from low-mass stars.

Table 1 summarizes the relevant optical data for the 214 cluster members present in our survey; rotational data are from Soderblom et al. (1993). Figure 1 shows the magnitude distributions of Pleiades stars in our survey. Also shown for comparison is the magnitude distribution in the central region of the field of view (FOV, dashed line; this region provides superior X-ray information, not only because of its greater effective area, but also because the angular resolution of the ROSAT mirror is much better closer to the telescope axis). In total, 44 (of 214) Pleiades members fall within the central field of view (offaxis angles $< 20'$).

3. X-RAY DATA SELECTION AND ANALYSIS

An image of our deep PSPC exposure of the core of the Pleiades cluster is shown in Figure 2, and the main characteristics of the observation are summarized in Table 2. The total observation is comprised of data from two observing 'seasons', $\sim$ 6 months apart. During the first period the satellite was operated in the normal 'wobble mode', with a peak-to-peak amplitude of $\sim$ 5 arcmin, while in the second period, the wobble amplitude was reduced to $\lesssim 1$ arcmin. During some (sub)segments of both periods the spacecraft wobble was completely suppressed.

The data obtained during this observation were first processed by the ROSAT Science Data Center with the Standard Analysis and Software System (SASS), and were subjected to further processing by us. In particular we have conservatively eliminated $\sim$ 11.6 ksec of the total observation[1] which showed significant enhancement in the background due to OV fluorescence (at 0.55 keV; cf. Snowden et al. 1994). Furthermore, comparison of the X-ray source positions (obtained separately by analyzing the two widely separated segments of our observation: 'A' & 'B'; cf. Table 2) with optical counterparts showed a difference in the boresight corrections for the two segments: While the source positions obtained from segment B match the optical positions closely (Δ R. A. = 0.3", Δ Dec = 1"), those in segment A are systematically offset by $6.5''$ and $9.5''$ along the X and Y directions, respectively. We have therefore assumed that the data in segment B are essentially on the same spatial registration as the optical data, and that the photon positions in segment A must be shifted to match that of segment B. Hence we have transformed all the source positions to the 'optical' positions.

Given the screening of the observation time we have performed, we have also recomputed new exposure maps. We have separately computed the maps relative to segment A and B, shifted that obtained for segment A to match the shift in the data, and summed the two maps. Finally, we compute the exposure at a given source position by averaging over the nearest neighbors of the pixel which corresponds to the source position. Since the instrument maps which are used to construct the exposure maps already have information regarding the window support structure and mirror vignetting in them, no additional corrections are needed for these effects.

3.1 Detection Method

Since we have screened the SASS data, we have chosen not to use the standard list of X-ray sources produced by SASS. Moreover, none of the currently available automated

[1] The complete list of retained times, needed to reproduce present results, can be obtained from the authors.

detection techniques, such as that of MIDAS/EXSAS (Zimmermann et al. 1993) or of IRAF/PROS (Worrall et al. 1992), is suited for crowded fields such as the Pleiades: errors in the count determination arise both from confusion due to unresolved sources and from the failure of the algorithms to correctly identify 'clustered,' but resolved, sources. We have therefore developed a detection scheme to handle these and other problems (see Appendix Appendix A; also, Kashyap et al. 1994).

We have found for our Pleiades field that the EXSAS detection algorithm (which incorporates Local, Map, Maximum-likelihood Detection algorithms in sequence, plus a source matching/merging step) produces a more comprehensive list of unique sources than the PROS algorithm (Local Detect plus matching/merging). However, the EXSAS algorithm misses a few obvious sources that are indeed recognized at high S/N by PROS, and there are a handful of cases where both EXSAS and PROS miss sources which are evident to the eye, probably because of the mismatch between the strong variation of the size of the Point Spread Function (PSF) and the fixed size of detection cell(s).

Based on the above findings, we have decided to adopt the list of (129) sources produced by the EXSAS detection algorithm (with a likelihood ≥ 8) as the starting point in the construction of a master list of possible X-ray sources. To this we have added 10 sources found only by PROS LDetect, and the 15 found with $S/N > 3$ at Pleiades optical positions. In this manner we obtain a list of 154 candidate X-ray sources for which counts are obtained as described in Appendix A and in Kashyap et al. (1994). Application of a $S/N > 3$ criterion yields a final list of 102 X-ray sources. For undetected Pleiades stars, we have evaluated the 3σ upper limits to their X-ray counts.

Both detections and upper limits have been computed in the 20-201 PI channel bandpass. The lower boundary has been adopted to exclude the softest channels where the PSPC suffers from the so-called electronic ghost image problem (Nousek & Lesser 1993) that dramatically affects the low energy instrument map. The upper limit at the PI channel 201 is applied because no instrument map (necessary to build the exposure map) is available above this energy.

3.2 Identifications of Pleiades X-ray Sources

In order to identify the detected X-ray sources, we have adopted identification criteria that take into account the degradation of spatial resolution with off-axis angle: we divide the FOV into three annular regions and adopt a source–identification circle with radii held constant in each region. In the inner region (off-axis angles $\theta \leq 20'$), where the instrument achieves the best angular resolution, we adopt $r_{id} = 30''$ as the radius of the identification circle; in the middle region ($20' < \theta \leq 30'$), $r_{id} = 60''$; and in the external region ($30' < \theta \leq 50'$), $r_{id} = 120''$. We discard the region of the FOV beyond $\theta = 50'$ because of the enormously increased width of the PSF and its strong departure from circular symmetry.

We identify a total of 79 X-ray sources with at least one Pleiades member: 65 X-ray sources have only one Pleiades star in the identification circle, 10 sources have two possible counterparts, and two sources have three Pleiads in the error circle; the remaining two X-ray sources are actually due to a complex overlap of two or more sources, and are treated as described in Appendix A. In this manner, we are able to identify 101 of the 214 Pleiades stars in the FOV[2]. However, based on previous observations, we have discarded the identification of 2 of these stars as X-ray sources. In the case of the X-ray source at ($3^h\ 49^m\ 41^s.2$, $24^\circ\ 18'\ 42''$), which has both the Pleiades star Hz2366 and the Hyades star Hz2411 in its error circle, we attribute the emission to the Hyades star; this star has a smaller X-ray–to–optical position offset and is physically closer to us. We therefore consider the observed rate as an upper limit to the emission of the Pleiades star. This choice is consistent with the observation of Stauffer et al. (1994), in which the same sources lie close to the center of their FOV and hence are resolved. In the case of the X-ray source at ($3^h\ 45^m\ 40^s.5$, $24^\circ\ 37'\ 30''$), we attribute the emission to the star Hz727, despite the presence of the star B203, on the basis of IPC data (Paper I) that allows us to resolve the two stars. In all other cases we split the observed emission in equal parts between the possible counterparts. Table 3 summarizes the number of identifications in each region of the FOV.

The identification process described above leaves 23 X-ray sources not identified with any known Pleiades members. Of these 23, we have identified 6 with objects from the SIMBAD catalog (supplied as a ROSAT 'Data Product,' see Table 4a). Of the remaining 17, we have identified 10 with very faint stars after an extensive search in the literature; because of the faintness of these stars, reliable probabilities of their cluster membership cannot be computed. Relevant optical information for these stars is summarized in Table 4b.

In summary, we detect a large fraction of the surveyed stars of all spectral types, especially later type stars; in particular, in the central region of the field where the spatial resolution and sensitivity of the instrument is highest, we detect all but one of the stars later than $\sim$ F7 (cf. Figure 3).

We have computed the probability p of identifying an X-ray source with an unrelated

[2]As matter of fact, 90% of the identifications have offsets (between X-ray positions and optical positions) of less than $10''$, $35''$, $100''$ in the three regions, respectively. These values reduce to $8.5''$, $28''$, and $33''$ if we consider only those identifications which have single optical counterparts to the X-ray sources.

Pleiades star as:

$$p = \frac{\pi r_{id}^2}{A} N_* , \tag{1}$$

where N_* is the number of optical cataloged stars present in each region of the FOV (44, 34, 136 for the three regions in the FOV, respectively), and A is the area in which the identification circle radius is equal to r_{id}. The number of expected spurious identifications are 0.24, 0.43, and 3.3 for inner, middle and external regions, respectively.

3.3 Count Rate, Flux, and Luminosity

The count rate in the 0.2-2.01 keV passband has been evaluated by dividing the net source counts by the effective time computed from the exposure map at the source position.

To evaluate the conversion factor between counts to flux, we have assumed a simple 1-temperature Raymond-Smith thermal spectrum model and a value of $N_H = 10^{20.3}$ cm^{-2} (Bohlin, Savage, & Drake 1978) for most stars (see below). For purposes of comparison with *Einstein* Observatory surveys (Paper I) we have evaluated this count-to-energy conversion factor (*cecf*) to get source flux in the 0.16-4.0 keV bandpass. Since the *cecf* depends on assumed coronal temperature, we have estimated individual source temperatures from the hardness ratio. For this purpose we have computed the hardness ratios

$$HR = \frac{Counts(0.2 - 0.9 \text{ keV})}{Counts(0.9 - 2.01 \text{ keV})} . \tag{2}$$

The values of HR have been individually corrected for the vignetting energy dependence and for non-uniformities of the PSPC using the values of the exposure maps at source position in the various energy bands considered. The median value of the deduced *cecf* is 1.21×10^{-11} ergs cm^{-2} ct^{-1}, with 90% of the values differing no more than 20% from the median. We consider this dispersion (20%) as the typical error introduced by our procedure in the determination of the *cecf*. In deriving upper limits to the flux of undetected Pleiades members we have used the value of the median of the *cecf* deduced for detected stars.

We have adopted a value of $N_H = 10^{20.3}$ cm^{-2} for all but 18 stars falling in our sample that Stauffer & Hartmann (1987) report with $E(B-V) > 0.1$. For these stars we have computed the conversion factor from the corresponding N_H.

A further source of errors is due to the presence of differential reddening across our FOV (Breger 1987). Measurements of color excesses for individual stars in our sample exist for only 50 out of 214 stars in our catalog and only for these 50 stars we can obtain conversion factors taking into account the absorption along the individual line of sight. Without individual measurements of $E(B-V)$, we can underestimate the

X-ray luminosity for heavily reddened stars by up to a factor 3-5, depending on the emitted spectrum.

We have evaluated the overall uncertainty due both to the assumption of a source model spectrum (single temperature vs. double temperature Raymond-Smith) and to our ignorance of interstellar hydrogen column by performing a two-temperature fit with the absorption as a free parameter for the stars with more than 200 counts. Results indicate that in *extreme* cases, the resulting fluxes can differ by up to 50% from those obtained with our 'standard' procedure. Although this test has been possible to carry out only for the most intense sources, it does give an estimate of the overall uncertainty introduced by our flux determination procedure.

X-ray luminosities have been computed assuming a common distance of 127 pc (Crawford & Perry 1976) for the cluster members. The estimated uncertainty on the luminosity due to individual cluster member distance is $<15\%$. Hence the overall uncertainty in the computed luminosity is $\sim 60\%$ for 3σ sources and is dominated by the errors in count-to-flux conversion.

We summarize the X-ray data for all the Pleiades members in our FOV in Table 5; upper limits have been computed for the X-ray emission of the 115 Pleiades members which have not been identified with any X-ray source. The X-ray data for identified field stars are summarized in Table 6a. The X-ray data for the 10 potential faint cluster members are listed in Table 6b. Table 6c gives the positions and count rates of the 7 unidentified X-ray sources.

3.4 Comparison with previous surveys

The Pleiades Cluster has been previously surveyed in the X-ray using both the *Einstein* Observatory and ROSAT. A summary of overlaps in surveyed stars and X-ray detections between these surveys and the observations described here is given in Table 7. In the following we will summarize in detail the comparison of our observation with other PSPC observations.

The Pleiades cluster was observed with the PSPC as part of ROSAT All-Sky Survey (RASS), conducted between July 1990 and January 1991 (Schmitt et al. 1993). The RASS data allowed the detection of 24 X-ray sources in the core region of the Pleiades cluster with a likelihood > 8, and these detections have been identified with 28 Pleiades member stars. Of these 28, 15 lie within the region observed by us, and we detect all 15 in our survey.

Three of the 15 common detected stars have count rates in RASS that are more than a factor of 2 greater than measured by us. One was observed in RASS during a flare (Hz2034); another is the brightest of a group of X-ray emitting Pleiades stars not completely resolved in the RASS and in our survey (Hz686), and hence the rate reported by Schmitt et al. is likely to be affected by contributions from other nearby X-ray emitting stars; the last (Hz1234) is suspected to be variable (cf. Stauffer et al. 1994). The limiting sensitivity of the RASS was $\sim 4 \times 10^{29}$ ergs s^{-1} at the distance of the Pleiades; in our sample, 4 stars undetected in the RASS have X-ray luminosities at least twice this value (i.e., $L_x \geq 8 \times 10^{29}$ ergs s^{-1}): Hz563, Hz625, Hz738, and Hz1136. Only one (Hz563) has shown evidence for variability; it is dimmer by a factor of 2 also in the *Einstein* survey. The remaining 3 stars, have $N_H \geq 10^{21} cm^{-2}$ based on their $E(B-V)$, and may have had count rates below the RASS threshold despite their higher intrinsic luminosity.

Another ROSAT PSPC survey of the Pleiades cluster was carried out during the pointed phase of the mission, contemporaneously with our observations (Stauffer et al. 1994): Pointed observations of 3 fields with exposures in the 20-26 ksec range were carried out, mostly in August and September of 1991, with short segments in August 1992 and February 1991. The central field of Stauffer et al. has a large area overlap with our field; regrettably the satellite had severe pointing problem during this observation, making it difficult to estimate the 'true' observation time of a given source and its flux determination.

In most cases, the count rates (or upper limits) for the common stars as determined by Stauffer et al. lie within a factor of 2 of the rates (or upper limits) measured by us. However, 21 stars have rates that differ by more than a factor of 2. In all but 2 of these cases (Hz762 and Hz1094), the star in question happens to lie beyond an off-axis angle of $20'$ in the observations of Stauffer et al. (i.e., beyond the central regions of the PSPC), and in 10 of the 13 cases for which measurements from the other pointings of Stauffer et al. with smaller off-axis angles is available, the difference between our and Stauffer et al.'s measurements are smaller, differing by less than a factor of 2. Hence, we assign most of the apparent variation in count rates and number of detections to differences in count rate determination and the adopted source existence criteria, and suggest that a homogeneous analysis of both the Stauffer et al. and our data sets would resolve most of these discrepancies. Until such an analysis is carried out, it is of course not possible to make definitive statements about short timescale variability based on these data.

Finally, we note that the observations and analysis described here differ from the above ROSAT surveys in the following respects: (1) our observations are much more sensitive than those carried out during RASS; (2) the regions of the Pleiades Cluster observed by Stauffer et al. (1994) and by us differ not only spatially (the center of our field being $15'$ away from the center of their 'central' field), but also in terms of the intra-cluster medium; (3) given the pointing problem of the Stauffer et al. central field, in this sky region our data have a better 'quality'; (4) our analysis procedure differs from that of Stauffer et al. in that it allows us to extend the analysis region to PSPC off-axis angles of 50′, and also gives us a uniformly determined set of count rates with minimal internal variations (cf. Fig. 2 of Kashyap et al. 1994). If we had adopted the Stauffer et al. approach (assuming one were able to collect 99% of the source counts) we would have systematically underestimated source intensities (by up to 30%) and the S/N of the sources detected outside the central part of the field of view. However the relevance of this effect is substantially reduced for sources detected in the central part of the field of view.

4. STELLAR X-RAY LUMINOSITY FUNCTIONS

Einstein observations showed (Paper I; Feigelson & Kriss 1989; Vaiana et al. 1992; Damiani et al. 1995) that the X-ray luminosity functions for stars of distinct clusters of different age are systematically shifted with respect to one another; furthermore, luminosity functions for stars in individual clusters have a smaller spread than the corresponding luminosity functions for field stars, whose age range is wider (see for example Figure 5c of Paper I). This implies that stellar age is a key factor in determining stellar X-ray activity levels. The results obtained with the *Einstein* data are however limited by severe censoring. Because of this censoring, the observed variance in X-ray luminosity is only a lower limit to the 'true' variance; and for this reason, it is not certain that the difference in variance between the field stars and individual clusters is due to their difference in age distributions rather than to heavier censoring of cluster data. In order to resolve this issue, it is necessary to obtain very deep exposures of young stellar clusters, thereby allowing us to reach stellar X-ray luminosity levels comparable to those of nearby field stars, and thus obtain comparable censoring levels for field stars and those clusters. This is what we proceed to do in the following.

As in Paper I, we consider subsamples of stars in five separate ranges of colors: $(B-V)_0 \leq 0$ (B stars); $0 < (B-V)_0 \leq 0.5$ (dA and early dF stars); $0.5 < (B-V)_0 \leq 0.8$ (late dF and dG stars); $0.8 < (B-V)_0 \leq 1.45$ (dK stars); and $(B-V)_0 > 1.45$ (dM stars). In addition, the reddest dM stars (from Hambly, Hawkins, & Jameson 1993) are considered separately from the last category of dM stars. Our analysis procedure follows the usual method of constructing maximum likelihood luminosity functions (MLLF) for censored data (Avni et al. 1980; Schmitt 1985; Feigelson & Nelson 1985), and bootstrap techniques to evaluate the errors on their means and medians (Schmitt 1985). The MLLFs thus obtained are plotted in Figure 4 for each subsample defined above (except for B stars). The means and medians summarizing the luminosity functions are given in Table 8.

4.1 B stars

One of the questions left open by previous X-ray observations was whether late B and A type stars do produce X-ray emission, or whether the small number of detections in this range of spectral types is instead due to unresolved companions of these stars (Schmitt et al. 1985; Caillault & Zoonematkermani 1989; Grillo et al. 1992).

In the present survey we detect 4 of 17 B stars (1 of 4 in the central region) down to $L_x = 10^{28.5} ergs\ s^{-1}$, essentially the same fraction as the *Einstein* survey. All the detected B stars are known or suspected binaries. We obtain no new detections in this spectral type with respect to those of *Einstein*, and we quote an upper limit for the star Hz 1432 (η Tau) of $L_x = 10^{28.86}$ ergs s^{-1}, incompatible with the detection at $L_x = 10^{29.60}$ ergs s^{-1} obtained from the *Einstein* survey. Since the S/N ratio of the *Einstein* detection was very near the acceptance threshold, it is possible that it was a spurious detection. Stauffer et al. report a value of $L_x = 10^{28.71\ (\pm 0.12)}$ ergs s^{-1} for η Tau, consistent with our upper limit. They note, however that this source may result from the combination of two distinct sources.

The lack of new detections in this color range, in spite of the fainter limiting sensitivity reached, is consistent with the existence of a high luminosity tail populated by a small number of detected stars, and of a body of the distribution with a much lower X-ray emission level, i.e. with a 'bimodal' distribution, as already noted by Stauffer et al. (1994) with comparable sensitivity observations. The occurrence of this tail can be fully explained as a result of unresolved late-type X-ray emitting companions, even if other explanations cannot be ruled out: Mermilliod et al. (1992) report a multiplicity fraction of 0.4 for F5-K0 stars in the Pleiades, and our results are consistent with this observation. Assuming that all detections of X-ray emission from B stars are really due to later type companions, we can place a lower bound of $\sim 25\%$ on the number of multiple systems. Small number statistics, and our lack of knowledge of the distribution of secondary masses for B star primaries, do not allow us to draw firmer conclusions.

4.2 dA and early dF stars

One of the outstanding questions of stellar activity research is the relation between coronal X-ray emission and convective activity: It is certainly a central tenet of the 'standard' model for stellar activity of late-type stars that convection is a prerequisite for the existence of coronal X-ray emission. The obvious, and often-applied, test of this assertion is to determine the X-ray properties of dA and early dF stars, and in particular to determine the activity level of stars which stellar evolution models predict to have no (or very weak) convection layers (cf. Schmitt et al. 1985).

The mass at which the surface convective activity thought to be responsible for magnetic dynamo activity sets in on the Zero Age Main Sequence corresponds to spectral type $\sim$ F0 ($B - V \sim 0.21$; Mihalas 1978; Gilman 1980). There are 21 stars in the range $0 < B - V \leq 0.3$ and 16 stars in the range $0.3 < B - V \leq 0.5$ in our optical sample. Of the former 21 (dA and early dF stars), 5 are 'detected,' with L_x ranging between 10^{29} and 10^{30} ergs s^{-1} in our survey; and of the latter 16 (dF stars), 9 are detected as X-ray sources (see Figure 4a).

Given the 'detection' of 5 dA stars, the question of whether unseen companions to these A stars are responsible for the A star X-ray emission demands resolution. Of these 5 detected stars, 4 are known to be binaries, while the star Hz1384, one of the more intense (and steady) X-ray emitters in the Pleiades, does not show any signatures for the presence of companions (see for example Mason et al. 1993). Its X-ray luminosity as measured by us (as well as Schmitt et al. 1993 and Stauffer et al. 1994) is essentially at the same level as observed with *Einstein* (for a detailed discussion of this star see Paper I).

4.3 dG Stars

We detect 24 of 37 dG stars in our FOV; all 16 stars in the inner and middle regions. These 16 stars span a range of X-ray luminosity of roughly one and half orders of magnitude, with $L_x \sim 10^{29} - 10^{30.5}$ ergs s^{-1}. All the detections and upper limits obtained in the external region are consistent with these values. Further, the MLLF obtained for the entire sample of dG stars (cf. Figure 4b), is very similar to the MLLF obtained for the sample of dG stars in regions 1 and 2. The strong similarity of these two functions leads us to conclude that the MLLF obtained for these stars is very close to the 'true' luminosity function, and that the observed range in L_x thus characterizes the spread in the activity level of a sample of stars with a well-defined age and homogeneous metal composition. Based on this conclusion, our data confirm that the luminosity function for dG stars in individual clusters has a smaller spread than the corresponding luminosity functions for dG field stars. It is possible that the homogeneous reduction of all the pointed data of the Pleiades obtained by ROSAT (which would increase the sample size by a factor 2 or 3) would allow a better determination of the shape of the luminosity function and provide further information on the origin of the spread.

We have verified that the binary dG stars are more intense X-ray emitters than single dG stars. However, unlike Hyades dK stars (Pye et al. 1994), the X-ray luminosity function of the Pleiades dG binaries is consistent with that obtained by the convolution of the single dG star luminosity function with itself.

4.4 dK Stars

We detect 42 of 76 dK stars present in our FOV; and 28 of 31 stars present in the inner and middle regions. The MLLFs for both the entire dK star sample and for the 31 dK stars in regions 1 and 2 are shown in Figure 4c, and show (as with dG stars) that this determination of the luminosity function should be a good approximation of the 'true' luminosity function. The observed spread in L_x is slightly larger than an order of magnitude, but is definitely smaller than that for Pleiades dG stars and young disk population dK stars (cf. Barbera et al. 1993). We also note that the star Hz1136, whose 'superflare' (Caillault & Helfand 1985) was responsible for the extended high luminosity tail in the *Einstein*-derived MLLF, has been detected in the ROSAT observation with a luminosity level about one order of magnitude below the *Einstein* value.

The X-ray luminosity function of the known Pleiades binary dK stars is consistent with the convolution of the Pleiades dK single star luminosity function with itself. Hence in the case of the Pleiades the presence of the binaries does not account for a major portion of the observed spread of the dK star X-ray luminosity function; this is unlike the Hyades, in which the observed difference in the X-ray luminosity level of the single and binary dK stars explains half of the observed spread in the X-ray luminosity function. The spread of the X-ray luminosity functions of the Pleiades binary dK stars is of the same order of magnitude as that observed in the Hyades binary dK stars ($\sim$ 0.7 dex) by Pye et al. (1994), while the Pleiades 'single' dK stars show a spread of the X-ray luminosity level larger than that observed among the Hyades dK stars. Thus, X-ray luminosity evolution of both single and binary stars appears to be similar for ages up to $\sim$ 70 Myr, and differs substantially afterwards, perhaps due to different rotational evolutions of the binary and single stars. These findings are consistent with the interpretation that while up to the Pleiades age the evolution of X-ray luminosity levels of single and binary stars is quite similar, the L_x evolution with age for single stars becomes more rapid than for binary stars at ages lying between those of the Pleiades and of the Hyades.

4.5 Early dM Stars

The *Einstein* survey was able to detect only 10% of the cataloged dM stars, and it remained unclear whether these detected stars were exceptional objects or the tail of a distribution function whose main portion fell just below the observational threshold. Thus, the trend of decreasing X-ray luminosity with increasing age detected with *Einstein* observations could not be extended definitively to low mass stars. With this deep ROSAT exposure we have the opportunity to explore a range of X-ray luminosity typical of young field stars (Barbera et al. 1993) in a very young cluster. In total, we detect 15 of 47 dM stars present in the entire FOV; a much larger fraction of dM stars (7 of 9 stars) in the central $30'$ radius region of FOV; and all 4 present in the central $20'$ radius region where the instrument has the highest sensitivity. The MLLF we obtain is shown in Figure 4d. The observed spread in the L_X level of Pleiades dM members is $\sim$ 1.5 dex, slightly lower than $\sim$ 2 dex spread observed in the case of the young disk early dM stars (Barbera et al. 1993).

Based on this deep observation, we conclude that the dM stars detected by *Einstein* and the dM stars detected by ROSAT in the external part of FOV are the tail of a luminosity function that spans about one-and-a-half orders of magnitude, with $L_x \sim 10^{28.5} - 10^{30}$ ergs s^{-1}. Implications of this result are important for the origin of the X-ray background near the Galactic Plane (the so-called Galactic Ridge), where the contribution of young stars has been shown to be relevant (Micela 1991; Vaiana et al. 1992).

4.6 Very Faint M Stars

The discussion in the previous section was concerned with only early dM stars (up to $\sim$ M5) because of the incompleteness of the optical catalog at faint magnitudes. In the present section, we discuss the X-ray properties of late dM stars using the Hambly, Hawkins, & Jameson (1993) catalog, which includes all stars up to $m_I \sim 18.5$ in the core of Pleiades with proper motion consistent with that of the cluster. Since, as already discussed, this sample may be heavily contamined by field stars, we analyze it separately from the stars in our Pleiades catalog. We note, however, that there is an overlap between our and the HHJ catalogs.

A total of 116 HHJ stars fall in our FOV. After the identification process, 25 of the 116 fall within the identification circles of X-ray sources, of which 8 are uniquely identified with X-ray sources, 6 are already present in our catalog, and the rest fall within identification circles of sources already identified with other cluster members.

If we assume that all 25 (of 115) stars are X-ray emitters, we would deduce a detection rate of 21.5%, which increases up to 40% (10 of 25 stars) in the central region of the FOV. These fractions are smaller than those obtained for the other spectral types. The apparent decay of the detection rate with spectral type may be due to an increase of field star contamination with increasing magnitude: Because field stars are on average considerably older than Pleiades stars, contamination of Pleiades stars by field stars would introduce a stellar population with systematically lower X-ray luminosity than Pleiades members, if the correspondence between X-ray luminosity and age holds also for these faint stars. Adopting the magnitude of such contamination as estimated by HHJ for bins of m_I, and assuming that all contaminating stars are undetected, we can evaluate the upper limit to detection rates in each magnitude bin. We compute the detection rates corrected for field star contamination (cf. Table 9) for different values of m_I; the detection rate appears to decrease towards later spectral types, indicating a decrease of typical X-ray luminosity level with decreasing stellar mass. We note, however, that the surface flux for the detected late dM stars is much higher than that of earlier spectral types. Furthermore, we note that we have 7 unidentified sources (see

§3.2) whose presumably optically faint counterparts may increase the detection rate for very low mass stars.

Our analysis is in agreement with the recent work of Hodgkin et al. (1995), who have conducted an analysis of chromospheric and coronal activity of low mass stars in Pleiades. These authors conclude that at I $\sim$ 14, Pleiades stars have, on average, less efficient dynamos or heating mechanism, with some stars being a very strong emitter.

5. VARIABILITY OF X-RAY EMISSION

Our current understanding of stellar X-ray emission is based on the 'solar analogy,' which posits that hot plasma within coronal magnetic loops is the main source of stellar X-ray emission, as on the Sun. Observations of solar X-ray emission show that X-ray emission on the Sun is subject to considerable variability, on time scales ranging from less than an hour (flares) to the 11-year duration of the solar cycle (cf. Vaiana & Rosner 1978). Detection and understanding of similar variability on other stars is therefore of significance to both validating and extending the 'solar analogy' and, by implications, probing the mechanism of X-ray production on the Sun itself.

Numerous stars (both on the main sequence and on the giant branch) have been observed to flare with the *Einstein*, *EXOSAT* and ROSAT Observatories: Indeed, three stars in our data set have flared during our ROSAT observation (HCG144, HCG307 and HHJ435/Hz892; cf. Sciortino et al. 1994). However, opportunities for observing longer timescale variations had been generally lacking until the advent of the ROSAT Observatory. Here, we focus on the qualitative aspects of such longer duration observations, and relegate studies of individual flares and quantitative analyses of the general variability to a follow-up paper. We first consider the variation in X-ray emission observed over the half to one year timescale allowed by the ROSAT Mission itself, and then discuss the longer period comparisons between *Einstein* and ROSAT .

5.1 Half-year timescale

Our observations of the Pleiades Cluster were performed in two separate long duration segments (cf. Table 2), roughly 6 months apart. This circumstance allows us to explore the variability of X-ray emission in this hitherto unexplored region of the variability parameter space.

We have compared the count rates obtained in the two segments of our data set for the 77 X-ray sources identified with Pleiades members (cf. §3.2; we have ignored the Pleiads identified with the two complexes of X-ray sources whose individual rates have been computed according to the reconstruction procedure described in appendix A) and for the 10 possible Pleiades members as listed in Table 4b. With the exception of 3 stars whose emission has varied by more than a factor of 2, and 3 stars which have varied by about a factor of 2, we find (cf. Figure 5) that the remainder of the stars in our sample ($\sim 90\%$) have essentially identical emission levels. This result is verified when a more sophisticated analysis based on a comparison of the observed and the maximum likelihood count rates (Sciortino & Micela 1992) is performed on the data set. With this analysis, which takes into account exposure time at the position of the source, detection information, and count statistics to test for the existence of a source rate compatible with the observed rates, we find that there is no evidence that (except for flares) the X-ray emission of Pleiades stars changes significantly over the half-year timescale considered here. Indeed, in only about 10% of the Pleiades stars (noted above) do we find variability at a confidence level $> 3\sigma$ on the 6-month timescale. Note, however, that amplitudes variations smaller than a factor of 2 cannot be detected with available data.

Thus, given our paradigm of stellar X-ray emission (viz., the 'solar analogy'), the lack of observable modulation in the X-ray emission of Pleiades stars suggests strongly that these stars are so active that at any given time most of their surface is covered by coronal structures. (The alternate possibility - namely that the stars are in an activity minimum state- is eliminated by virtue of the fact that these stars are very X-ray active). Note, however, that this does not imply that the emission is 'saturated' (cf. §6.2).

5.2 Ten-year timescale

The Pleiades cluster was observed with *Einstein* between 1979 and 1981 (cf. Paper I), and by ROSAT in 1990 and 1991, therefore giving us a decade-long baseline to determine variability in X-ray emission from young main sequence stars. Previous studies have compared the X-ray emission level of the Pleiades members as measured by the *Einstein* Observatory (Micela et al. 1988) and by ROSAT. Schmitt et al. (1993) report extreme variability, from a factor 3 up to one order of magnitude, in a few Pleiades stars. They also show that, in the absence of intrinsic variability, the ratio of the IPC and PSPC count rates for the Pleiades stars should be ≈ 0.45. From their determination of the maximum likelihood distribution of the IPC/PSPC count rate ratio (shown as the solid stepped line in their Fig. 6), one can deduce that about 20% of the Pleiades stars in their sample have changed their X-ray emission level over a ten years time scale by more than a factor 2. As noted by Schmitt et al., about half of these 'variable' stars show evidence for a flare during one of the two epochs in which they were observed. Stauffer et al. (1994) report (see their Fig. 7) that 20 out of 135 Pleiades stars (i.e., approximately 15%) have changed their emission by more than a factor 2. Again, some of those variations can be explained by the occurrence of large flares.

The fraction of the Pleiades stars in our survey that have changed their emission level by a factor two is certainly greater than 15% (26 out of 178 members in common in the present and in the *Einstein* surveys). However, in all but 3 cases (Hz1136, which was observed with *Einstein* during a flare, and 2 others which were detected with *Einstein* and have not been detected here with ROSAT), the magnitude of the variation is consistent with being less than a factor of 5 (cf. Figure 6), and hence it is unlikely that this variability is one of the causes of the larger spread in X-ray luminosities found in the MLLFs.

While individual stars in the Pleiades Cluster have varied their X-ray emission level, the average X-ray emission of stars - as determined from their X-ray luminosity functions - seen by both *Einstein* and ROSAT has remained constant (Schmitt et al. 1993; Stauffer et al. 1994; Sciortino et al. 1994). This result confirms what we have implicitly assumed, namely that the X-ray emission of different stars is uncorrelated, and provides support for the supposition that *Einstein* and ROSAT have mutually consistent instrument calibrations.

We further note that much of the long-duration X-ray variability appears to be concentrated in dK stars (16 of the 26 have $0.8 < B - V < 1.45$). Whether this is simply due to the larger number of dK stars in our optical sample or due to an intrinsic variable affecting a subsample of dK stars is unknown.

6. DISCUSSION

6.1 Correlation of X-ray Luminosity with Rotation for Late-type Stars

Correlation between X-ray emission and rotation has been clearly demonstrated for slowly rotating solar-like stars (Pallavicini et al. 1981; Walter 1982; Walter 1983; Maggio et al. 1987), while it has been shown that the most active stars such as the fast rotators in Pleiades (Paper I; Caillault & Helfand 1985; Stauffer et al. 1993), the X-ray selected stars of the *Einstein* Medium Sensitivity Survey (Fleming, Gioia, & Maccacaro 1989) and of the Slew Survey (Schachter et al. 1994), and the Weak-line T Tauri stars in Taurus-Auriga (Strom 1990; Damiani & Micela 1995) do not follow the same relationship, showing evidence for 'saturation' of X-ray emission at large rotation rates. This change of behavior appears to occur for equatorial rotation speeds in the 10-20 km s^{-1} range.

The scatter plots of L_x versus $v\sin(i)$ for our Pleiades stars are shown in Figure 7a and 7b for dG and dK stars, respectively. It is evident that the best-fit regression line computed for dG stars within the central $30'$ region of the field-of-view (an essentially complete sample) is less steep than the so-called Pallavicini relationship (Pallavicini et al. 1981) derived for stars in the solar neighborhood; we obtain a regression of

$$\log_{10} L_x = 28.40(\pm 0.14) \ + \ 0.9(\pm 0.10) \cdot \log_{10} \, v\sin(i) \,. \tag{3}$$

There is however no clear evidence of dependence of L_x on rotation in the case of dK stars: the only indication of a possible link of X-ray activity and rotation is that a dominant fraction of X-ray upper limits is concentrated in the low rotation range. Indeed, *the X-ray activity level of the slow dK rotators ($v \sin i < 15$ km s^{-1}) is indistinguishable from that of the fast dK rotators* as deduced from a Wilcoxon test. In contrast, we do obtain a correlation between L_x and $v \sin i$ for our dG sample, notwithstanding the large spread in the $L_x - v \sin i$ correlation.

The spread in the X-ray luminosity functions cannot be explained in terms of dependence of L_x on rotation rate: For the dK stars, there is no evidence for an activity-rotation connection (possibly because of the effects of 'saturation'; see Vilhu & Walter 1987); for the dG stars, the spread of L_x (or equivalently, the surface flux F_x) at a given rotation rate is about a factor three larger than can be attributed to measurement errors ($\Delta L_x/L_x \sim 1$) or to variations attributable to random orientations of the rotational axes ($\Delta L_x/L_x \sim 0.5$). As an illustration of the effects of this difficulty, consider that roughly half of the dK stars with $v \sin i < 7$ km s^{-1} have L_x values comparable to those of the fast dK rotators; further note that none of the Pallavicini et al. (1981) stars with similar color, luminosity class, and rotational velocity has X-ray luminosity levels comparable to these fast dK rotators.

Stauffer et al. (1994) have noted a change in the spread of the luminosity functions of Pleiades stars as a function of color, and attribute the smaller spread in L_x they observe in the reddest stars to 'saturation'. They suggest that a large fraction of the reddest stars in Pleiades have not as yet spun down, and are still near the activity 'saturation limit'; in contrast, they posit that dG stars have already spun down and thus their X-ray luminosity values are well below the saturation limit, explaining why their X-ray luminosity function is broader. Our observations suggest that this interpretation may be incomplete. In fact the 'saturation limit' seems to be reached by virtually all the K stars, even by the slow rotators. This is shown by the presence of a high fraction of slow rotators at high luminosity level (Fig. 7b), which cannot be simply explained by random orientation of rotational axes, and by the fact that, based on the X-ray luminosity function, the minimum level is $\log(L_x) \sim 28.7$. We note that in the center of field of view, we have detected almost all (28 out 31) of the observed dK stars, including several slow rotators (cf. solid symbols in Fig. 7b). Furthermore we show in Fig. 8 the residuals of $\log L_x$ around the best fit regression line of Fig. 7a found for Pleiades dG stars. It is evident that the total spread of the residuals spans one dex, comparable with the spread observed in the dK stars (cf. Fig 7b). Since both of these spreads cannot be explained by uncertainties in the L_x determination, we conclude that *surface rotation in and of itself is insufficient to determine the X-ray emission level of young dG and dK stars.* One obvious explanation could be that the variability level of young stars is much larger than that of older (field) stars. However, as we have shown before, while variability by a factor two is present in at least $\sim 15\%$ of Pleiades stars, its amplitude is insufficient to explain the entire luminosity function spread we have observed. This suggests that some other age-dependent parameter influencing stellar dynamo efficiency (such as the gradient scale length for interior differential rotation) must produce the observed spread in the $L_x - v \sin i$ dependence in dG stars and the nearly total masking of this dependence in dK stars.

6.2 The Physics of 'Saturation' of Stellar X-ray Emission

The lack of dependence of L_x on rotational velocity, as is observed in K Pleiades stars, is commonly interpreted as an indication of 'saturation' (e.g., Walter 1983). In the following, we will address the underlying physics of the saturation process; as we shall demonstrate, simple physical arguments allow us to place a lower limit on the value of the magnetic field required to confine the coronal plasma.

The observations of 'saturated' coronal X-ray emission give the constraint that the average surface X-ray flux is bounded from above,

$$f_x \lesssim 10^{7.5} \text{ ergs s}^{-1} \text{ cm}^{-2}, \tag{4}$$

where the right–hand side is the estimated value of the average 'saturated' surface X-ray flux. The most obvious simple explanation for this 'saturation' - namely that 'saturated' stars have their entire surface covered with coronal structure (cf. Vilhu 1984) - has a fatal flaw: It fails to explain why the X-ray surface brightness (e.g. f_x) is bounded from above, since even for a coronal filling factor of unity, coronal structures can become brighter by simply increasing their gas pressure. The question is thus: why is the mean loop gas pressure bounded from above?

The simplest physical argument which leads to 'saturation' of stellar surface X-ray emission by bounding the loop gas pressure is based on the idea that the coronal gas pressure must be less than the pressure of the confining coronal magnetic fields (B),

$$p_{\mathbf{gas}} \lesssim B^2/8\pi . \tag{5}$$

There are two cases to consider: First, the case ('Case 1') in which the dominant emission comes from structures smaller than the coronal pressure scale height ℓ (defined below); second, the case ('Case 2') in which most of the emission comes from structures of order of, or larger than, the pressure scale height. In the following, we shall assume that the coronal 'filling factor' f, defined as the fraction of the stellar surface which is covered by X-ray emitting material, is equal to unity; if $f < 1$, then the lower bounds we find will be yet higher (as shown below).

For case 1, we can combine constraint (5) with the relation governing optically-thin emission from coronal plasmas and the statement that (for simplicity) all the emission comes from structures ('loops') of length L to obtain

$$n_e^2 \, \Lambda(T) \cdot L \sim 10^{7.5} \text{ ergs cm}^{-2} \text{ s}^{-1} \,, \tag{6}$$

where emission per unit measure $\Lambda(T)$ is given approximately by

$$\Lambda(T) \approx 10^{-23} \text{ ergs cm}^3 \text{ s}^{-1} \tag{7}$$

in the temperature regime $10^{6.3} \lesssim T \lesssim 10^{7.3}$ K in the $1 - 150 \mathring{A}$ passband (e.g., Kato 1976). If we now combine equations (4), (6), and (7) with the scaling law obeyed by quasi-static structures with $L \lesssim \ell$, $T \sim 1.4 \times 10^3 (pL)^{1/3}$ (Rosner, Tucker, & Vaiana 1978) and the perfect gas law for a fully ionized gas ($p_{gas} = 2 n_e k_B T$), we obtain

$$B \gtrsim 1.3 \times 10^2 (T/10^6 \text{ K})^{-1/2} \text{ G} \,. \tag{8}$$

For case 2, we can estimate the average coronal emission properties by using the fact that most (e.g., $\sim 90\%$) of the (optically–thin) emission actually comes from the first pressure scale height ℓ, i.e., that

$$n_e^2 \Lambda(T) \cdot \ell \approx 0.9 \times 10^{7.5} \text{ ergs s}^{-1} \text{ cm}^{-2} \,, \tag{9}$$

where $\ell = 6 \times 10^3 \; T \cdot (M_*/M_\odot)^{-1} (R_*/R_\odot)^2$ cm is the pressure scale height for a main sequence star with mass M_* and radius R_*. Then again using the perfect gas law, relations (7) and (9), and with a bit of algebra, we obtain a bound on the confining coronal magnetic field for these large scale structures,

$$B \gtrsim 0.4 \; T^{1/4} \, (M_*/M_\odot)^{1/4} (R_*/R_\odot)^{-1/2} \text{ G} \,. \tag{10}$$

These results are obtained for unit 'filling factor' f; if $f < 1$, then the right-hand sides of both eqs. (8) and (10) are multiplied by a factor $f^{-1/2}$, so that filling factors less than unity lead to yet larger values of the minimum confining coronal magnetic fields. For example, for typical coronal temperatures $\sim 3 \times 10^6$ K, we obtain bounding coronal magnetic fields of the order of 75 $f^{-1/2}$ G (Case 1) or 20 $f^{-1/2}$ G (Case 2) for dK Pleiades stars, quite similar to values of solar coronal magnetic fields estimated from potential field extrapolations in solar active regions. These bounds on the confining magnetic field depend either not at all (Case 1) or very weakly (Case 2) on the mass of the underlying star. As a consequence, the existence of an upper bound on stellar surface X-ray fluxes indicates the surprising result that coronal magnetic fields on Pleiades-age solar–like stars must be rather similar in field strength to solar magnetic fields in regions of maximal X-ray emission. Our results also confirm one's intuition that for fixed emission levels, more compact coronal structures should be associated with larger coronal magnetic fields.

7. SUMMARY AND CONCLUSIONS

We have presented results from a new study of X-ray emission from Pleiades open cluster members: We obtained maximum-likelihood integral X-ray luminosity functions in selected color-index ranges, studied the correlation of rotation rate with X-ray luminosity, and analyzed the variability in X-ray emission at different timescales. We confirm many of the results of the previous X-ray surveys of this cluster obtained from *Einstein* data in the B-K spectral type range as well as from a contemporaneous ROSAT survey carried out by Stauffer et al. (1994). Taking advantage of the high sensitivity of ROSAT and the high spatial resolution of the PSPC detector in the center of the FOV, we have determined X-ray luminosity functions down to emission levels of 3×10^{28} ergs s^{-1}.

The present observations allow us to draw the following main conclusions:

1. B and A stars show two different populations of X-ray emitters, one for which we can determine only upper limits to their X-ray luminosity, and another with detectable emission likely due to unseen late-type companions. The fraction of binaries with early type primaries as determined from X-ray data alone is possibly smaller than the fraction of binaries with later type binaries, but the difference is not statistically significant in our data.

2. All Pleiades dG stars show an X-ray luminosity level within 1 dex of their mean, as seen from the maximum likelihood luminosity function we have derived for an essentially statistically complete sample of dG stars.

3. We detect almost all catalogued early dM stars in the center of the FOV, where the PSPC achieves the highest sensitivity; these stars have luminosity levels in excess of 3×10^{28} ergs s^{-1}.

4. The spread of the X-ray luminosity functions of the Pleiades dG, dK and early dM stars is smaller than that observed for field stars of the corresponding spectral types.

5. A total of 8 X-ray sources have been identified with faint stars in the HHJ catalog with proper motion consistent with that of the Pleiades: We propose these stars as likely Pleiades members. The rate of detections of optically very faint members appears to be lower than the corresponding rate for other (earlier) spectral types.

6. The Pleiades dG stars show an almost linear dependence of X-ray emission on rotation for rotational velocities up to 100 km s^{-1}, with a spread about this relation that cannot be attributed merely to random rotational axes orientations, to measurement errors, or to variability.

7. The Pleiades dK stars show weak (if any) dependence of X-ray luminosity on rotation. 'Saturation' of the X-ray luminosity for these stars is evident, together with a large spread of X-ray luminosity (~ 1 dex) for the slow rotators ($v \cdot \sin i \leq$ 15 km s^{-1}).

8. We find that, unlike the Hyades dK case, the X-ray luminosity functions of the Pleiades binary dG and dK stars are consistent with being simple convolutions of the X-ray luminosity functions of single stars with themselves. This result suggests that the evolution of X-ray luminosity level of single and binary stars is quite similar up to the Pleiades age and that it differs for stars older than the Pleiades. This effect may be related to the different rotational evolution of binary and single stars.

9. Our results strongly suggest that a hitherto ignored stellar parameter must play an important role in determining the X-ray luminosity level; stellar parameters such as spectral type and rotation rate do not suffice. This effect is noticeable for young stars, a population in which slow rotators can reach X-ray luminosities much higher than predicted on the basis of data for field stars with similar spectral type and rotation rate.

10. We find no evidence of significant variability (other than flares) in X-ray emission on timescales of ~ 1 yr or less, but, in contrast, we find that 38% (and not less than 15%) of the Pleiades stars have varied by more than a factor 2 over timescales of ~ 10 yr. The magnitude of this variability, usually much less than a factor 5, is not sufficient to account for the one dex spread in the luminosity functions.

Acknowledgments. We would like to acknowledge useful discussions with S. Serio, S. Snowden, G. Hasinger, and J.H.M.M. Schmitt. We thank D. Soderblom, who has made available his rotational data on Pleiades stars in electronic form, and Peter Wang for assistance with data analysis. V.K. wishes to thank the personnel at Palermo and CfA for their hospitality. This research has made use of the Simbad database operated at CDS, and NASA's Astrophysics Data System. This work was supported in part by NASA Contract NAS5-30934 (SAO) and NASA Grant NAG5-1794 (Univ. of Chicago), and from Agenzia Spaziale Italiana, Ministero della Università e della Ricerca Scientifica e Tecnologica and GNA-CNR.

APPENDIX A
DETECTION METHOD

Detection algorithms currently available (LDETECT in PROS, (L/M)-DETECT and Maximum Likelihood (ML) in EXSAS) have serious limitations in a field as crowded as the Pleiades:

Cell Size: Both PROS and EXSAS use a sweeping-cell method for finding sources, and in both cases, there is no provision for varying the adopted cell size ($30''$, $60''$, $120''$ in PROS, and an additional $240''$ in EXSAS) to match the spread of the PSF across the image. Thus, there are regions in the image where none of the choices is optimal. Further, due to the approximate shape of the assumed PSF (see below), source counts computed using cell sizes smaller than the appropriate PSF spread would be erroneous.

Validity of Detections: A comparison of the results of PROS and EXSAS ML methods show that the latter consistently finds sources correctly in a crowded field, unlike the former, which sometimes identifies two sources as one. EXSAS is also better at finding unique positions for sources found at different cell sizes (especially in the central $20'$ region). However, the EXSAS ML method appears to have inherent problems in that it misses obvious sources, perhaps due to a distribution of photons seen as 'abnormal' with respect to the approximate shape of an (incorrectly) assumed PSF.

Shape of the PSF: Versions of PROS and EXSAS available to us used a model for the PSF that is known to be somewhat inaccurate. While this is not a significant problem in the central part of the field, it leads to incorrect estimates of source counts at larger off-axis positions. Further, an incorrect representation of the shape of the PSF could cause the likelihood of detection of point sources to decrease.

Overlapping Sources: There is no provision in either PROS or EXSAS to find, or compute source counts, for overlapping sources. In the case of the Pleiades, this is a serious limitation.

For the above reasons, we decided to combine both PROS and EXSAS results to obtain an exhaustive list of X-ray source positions, which we then use in an IDL/IRAF based algorithm to estimate source counts, S/N, and (3σ) upper limits for both isolated and overlapping sources in a consistent and uniform manner. These procedures are described below.

A.1 Detection Algorithm

We use a method previously developed for the *Einstein* IPC (Harnden et al. 1984) and similar to that used in PROS LDETECT to compute source counts. The counts in a detect cell centered on the source (C) are compared with the counts in a 'background' cell (T), also centered on the source,

$$C = \alpha S \ + \ B, \text{ and } T = \beta S \ + \ rB, \tag{A.1}$$

where α is the fraction of the source counts S falling within the detect cell, β is the fraction of S falling in the background cell, r is the ratio of the areas of the background to the detect cell, and B are the background counts in the detect cell. The background and source counts,

$$B = \frac{(\alpha - \beta)C + \alpha Q}{\alpha r - \beta}, \text{ and } S = \frac{(r-1)C - Q}{\alpha r - \beta}, \tag{A.2}$$

where $Q = T - C$, the counts in the 'frame region' surrounding the detect cell, are obtained by solving Eqs. (A.1), along with their associated errors,

$$\sigma_B = \sqrt{\frac{(\alpha - \beta)^2 \sigma_C^2 + \alpha^2 \sigma_Q^2}{(\alpha r - \beta)^2}}, \text{ and } \sigma_S = \sqrt{\frac{(r-1)^2 \sigma_C^2 + \sigma_Q^2}{(\alpha r - \beta)^2}}. \tag{A.3}$$

The errors in C and Q are approximated as $\sigma_X = \sqrt{X} + 1$. The significance of a detection is evaluated as the ratio $S/N = S/\sigma_S$, and the threshold for detection at a specified S/N is obtained by computing S for which S/σ_S equals the threshold.

Our method differs from that used in PROS and EXSAS in that:

1. We use circular detect and background cells with radii that vary across the FOV to match the variation in the FWHM of the PSF.
2. Even though we use the older version of the PSF to determine the radii of the detect and background cells, we use the recently developed model of the PSF (Hasinger et al. 1993) to compute α and β, which are therefore expected to be more accurate.
3. We correct for small overlaps between adjacent sources by cutting a pie shaped region out of both the detect and background cells, and correcting the values of α and β as required. Our adoption of circular detect cells makes this correction mathematically trivial. Our method for dealing with large overlaps is described in the next subsection.

Of the 154 sources in the master list, 16 extend close enough to each other (28 at energies < 0.4 keV) that the 'pie'-correction mentioned above was necessary. In addition, two other sources were highly extended, and are due to large overlaps of unresolved sources (4 and 6 individual optical candidates, respectively).

A.2 Overlapping Sources

In cases where the overlap between suspected sources is significant we use a generalization of the method described above to determine individual source counts and associated errors. and we assume that the putative X-ray source positions are coincident with optical positions, and center the detect cells on these positions.

If there are N sources in the region of interest with source strengths S_i, then the counts in a detect cell centered on source i,

$$C_i = \Sigma_j \alpha_{ij} S_j \ + \ \rho_i B, \tag{A.4a}$$

and the counts in a frame region surrounding all the detect cells,

$$Q = \Sigma_j \beta_j S_j \ + \ B, \tag{A.4b}$$

where ρ_i are the ratios of the areas of the detect cells to the area of the frame region, α_{ij} are the fraction of the counts from source j falling on the detect cell centered on source i, β_j are the fraction of the counts from source j falling in the frame region, and B are the background counts in the frame region. The detect and frame regions are in general irregular in shape, necessitating a numerical integration of the PSF over these regions. Eqs. (A.4) constitute a set of N+1 equations in N+1 variables, and hence can be written as a matrix equation,

$$\mathbf{C} = \aleph \cdot \mathbf{S}, \tag{A.5}$$

where '$\cdot$' denotes matrix multiplication, $\mathbf{C} = [C_1,\ C_2,\ \ldots\ C_N,\ Q\ ]^T$ and $\mathbf{S} = [S_1,\ S_2,\ \ldots\ S_N,\ B\ ]^T$ are column vectors (the superscript T denotes a matrix transpose). Note that $\aleph_{i \leq N, j \leq N} = \alpha_{ij}$, $\aleph_{i \leq N, N+1} = \rho_i$, $\aleph_{N+1, j \leq N} = \beta_j$ and $\aleph_{N+1,N+1} = 1$, from Eqs. (A.4). Inverting the above equation, we obtain an estimate of the source strengths S_i, and the background in the frame region B. The variances of S_i and B are

$$\sigma^{\mathbf{2}}_{\mathbf{S}} = \mathbf{\Gamma^2} \cdot \sigma^{\mathbf{2}}_{\mathbf{C}}, \tag{A.6}$$

where $\mathbf{\Gamma}$ is the inverse of the matrix $\aleph$, and the squaring is carried out for each element individually. Note that in order to preserve the statistical independence of the C_i and Q, the detect regions and the frame region must not overlap each other.

Table 2: ROSAT Observations of the Pleiades Cluster Core

Parameter	First Segment	Second Segment
Observation ID*	RP200068	
Detector	PSPC 2(B)	
Filters	None	
Field Center:		
(R.A., Dec)$_{2000}$	(3^h 46^m 48^s,	$23°$ $54'$ $00''$)
($l_{\rm II}, b_{\rm II}$)	($166°$ $41'$ $38.3''$,	$-23°$ $42'$ $43.9''$)
Wobbling Mode	Normal	Reduced
Observation Date	Feb/Mar 1991	Aug 1991
Start of Observation†	21823921 s	38623072 s
End of Observation†	23809893 s	38709269 s
Number of OBIs	7	2
ON time [ksec]	15.780	27.296
Selected time [ksec]	11.312	20.423

* PI: R. Rosner

† As measured by the spacecraft clock

Table 3: Summary of Identifications

Region	Off-axis angles	Number of Stars	X-ray Sources	Identified Pleiades	Unique Identifications
1	$0' - 20'$	44	50	35	31
2	$20' - 30'$	34	24	25	15
3	$30' - 50'$	136	28	39	19
Total	$0' - 50'$	214	102	99	65

Table 4: (A) Field Stars Identified with X-ray Sources

Name	RA(h:m:s)$_{J2000}$	Dec($\circ$ $'$ $''$)$_{J2000}$	V
CSI +23-03437	3:46:42.0	24:04:00.1	15.10
CSI +23-03436	3:46:30.0	23:58:59.9	14.60
HD282974	3:47:09.9	23:46:57.7	10.20
HD23822	3:48:56.9	23:51:27.0	6.89
BD +23 555	3:48:46.0	23:31:30.0	10.70
V 339 TAU	3:48:01.0	23:29:35.9	14.50

Table 4: (B) Possible Cluster Members Identified with X-ray Sources

Name	RA(h:m:s)$_{J2000}$	Dec($\circ$ $'$ $''$)$_{J2000}$	V	R	I
HHJ 288	3:48:07.9	23:44:23.8	17.2	16.3	14.4
HCG 307					
HHJ 263	3:47:26.6	23:38:02.3	17.6	16.4	14.6
HCG 269					
HHJ 421	3:45:46.4	23:47:43.5	15.9	14.9	13.3
HHJ 363	3:46:04.3	23:55:41.3	16.7	16.2	13.9
HHJ 435	3:46:06.5	23:50:20.9	15.2	14.5	13.1
HHJ 257	3:46:55.8	23:56:24.7	18.4	17.0	14.7
HHJ 299	3:46:59.3	24:01:43.3	17.6	16.6	14.4
HHJ 427	3:47:25.3	24:02:57.5	16.1	15.2	13.2
Hz 994	3:46:21.0	23:59:03.3	15.0*	...	...
Hz 1576	3:47:47.5	23:54:28.9	14.4*	...	...

*Magnitude Photographic from Hertzsprung (1947)

Table 6: (A) X-ray Fluxes of Field Stars

Name	$\Delta R.A.$ [$''$]	ΔDec [$''$]	Off-axis [$'$]	CtRt	SNR	HR	$cecf$	$\log(f_x)$
CSI +23-03437	-0.6	23.9	10.5	1.77	3.39	2.33 ± 1.45	1.42	-13.60
CSI +23-03436	20.0	-0.4	6.2	12.86	12.3	1.04 ± 0.17	1.13	-12.84
HD282974	-5.9	-3.3	8.6	6.69	3.14	2.15 ± 1.60	1.93	-12.89
HD23822	-4.2	29.7	29.5	1.60	4.52	10.53 ± 8.69	1.38	-13.65
BD +23 555	-98.2	75.5	33.2	10.17	4.61	0.36 ± 0.22	1.45	-12.83
V 339 TAU	-36.7	-17.4	29.5	10.67	6.46	1.63 ± 0.46	1.36	-12.84

Table 6: (B) X-ray Luminosities of Possible Cluster Members

Name	$\Delta R.A.$ [$''$]	ΔDec [$''$]	Off-axis [$'$]	CtRt	SNR	HR	*cecf*	$\log(L_x)$
HHJ 288	-4.5	4.0	$20'.5$	12.71	5.68	1.37 ± 0.48	1.20	29.47
HHJ 263	-7.5	5.5	$18'.1$	4.32	3.82	0.86 ± 0.43	1.12	28.97
HHJ 421	-3.0	5.3	$15'.4$	4.24	4.67	1.88± 0.80	1.33	29.04
HHJ 363	1.5	2.4	$10'.1$	4.19	5.62	0.97± 0.33	1.13	28.96
HHJ 435	0.0	3.2	$10'.1$	20.75	13.79	0.53 ± 0.08	1.28	29.71
HHJ 257	-3.0	-3.1	$2'.9$	2.03	4.70	0.97 ± 0.41	1.13	28.65
HHJ 299	-6.0	-1.3	$8'.1$	2.39	3.58	0.33 ± 0.33	1.45	28.83
HHJ 427	0.0	0.3	$12'.4$	6.42	6.44	1.53± 0.42	1.24	29.19
Hz 994	-3.0	0.1	$7'.9$	2.30	3.95	0.72 ± 0.35	1.14	28.70
Hz 1576	-4.5	-4.1	$13'.5$	3.96	4.48	1.78 ± 0.81	1.30	29.00

Table 6: (C) X-ray Data for Unidentified Sources

RA(h:m:s)$_{J2000}$	Dec($\circ\ '\ ''$)$_{J2000}$	Off-axis	CtRt	S/N	$\log(f_x)$
3:46:03.9	23:57:46.7	$10'.8$	8.61	8.38	-12.98
3:46:06.6	23:53:38.2	$9'.5$	2.29	4.00	-13.56
3:46:23.7	23:55:39.4	$5'.8$	5.36	7.82	-13.19
3:47:09.3	24:03:06.5	$10'.3$	2.64	3.84	-13.50
3:47:24.2	23:54:03.7	$8'.3$	2.09	3.17	-13.60
3:47:39.1	23:33:56.6	$23'.2$	6.13	4.17	-13.13
3:48:07.2	24:16:34.0	$28'.9$	10.02	4.39	-12.92

NOTES:

The flux at Earth, f_x is computed for $cecf = 1.21 \times 10^{-11}$ ergs cm^{-2} ct^{-1}

Table 7: Overlap of Previous Pleiades Surveys with Our Survey

	Einstein Survey	ROSAT Surveys All-Sky	Stauffer et al.†
Pleiades Stars in common	178	15	142 (5)
Number detected in Survey	60	15	100 (5)
Number detected by us	89	15	77 (5)
Undetected Stars*	80	0	36 (5)
Number with > 2X variations	26	3	20 (1)

* These are the stars in common to both surveys which are left undetected in both surveys

† Numbers within brackets denote coincidence with potential Pleiades members

Table 8: X-ray Emission with Spectral Type

$B-V$	Log Mean $L_x[ergs\ s^{-1}]$	Log Median $L_x[ergs\ s^{-1}]$
$0.3-0.5$	$29.32(+0.07,-0.07)$	$29.20(+0.08,-0.001)$
$0.5-0.8$	$29.68(+0.09,-0.10)$	$29.25(+0.10,-0.03)$
	$29.74(+0.11,-0.13)^c$	$29.41(+0.09,-0.13)^c$
$0.8-1.45$	$29.35(+0.04,-0.04)$	$29.21(+0.13,-0.10)$
	$29.43(+0.03,-0.03)^c$	$29.28(+0.12,-0.06)^c$
>1.45	$29.14(+0.07,-0.08)$	$28.85(+0.21,-0.20)$

NOTES:

Errors quoted are 68% confidence limits from bootstrap analysis

Superscript c indicates results from the central part of FOV

Table 9: Detection Rates for Very Faint Cluster Members

m_I	N_{opt}	N_{det}	Membership Probability	Corrected* Detect. Rate
12-13	1	0	84%	0
13-14	16	10	96%	0.65±0.37
14-15	47	11	94%	0.25±0.11
15-16	37	2	93%	0.06±0.05
16-17	14	2	88%	0.16±0.16

* Errors obtained are from statistical uncertainties in N_{opt} and N_{det}.

REFERENCES

Avni, Y., Soltan, A., Tananbaum, H., & Zamorani, G. 1980, ApJ, 238, 1800

Bohlin, R.C., Savage, B.D., & Drake, J.F. 1978, ApJ, 224, 132

Breger, M. 1987, ApJ, 319, 754

Caillault, J.-P., & Helfand, D.J. 1985, ApJ, 289, 279

Caillault, J.-P., & Zoonematkermani, S. 1989, ApJL, 338, 57

Crawford, D.L., & Perry, C.L. 1976, AJ, 81, 419

Damiani, F., & Micela, G. 1995, ApJ, in press

Feigelson, E., & Nelson, P.L. 1985, ApJ, 257, 695

Feigelson, E., & Kriss, G. A. 1989, ApJ, 338, 262

Fleming, T.A., Gioia, I.M., & Maccacaro, T. 1989, ApJ, 340, 1011

Gilman, P. 1980, in IAU Coll. 51, Stellar Turbulence, ed. D. Gray. & J. Linsky, (Berlin: Springer), p. 19

Gorenstein, P., Harnden, F. R., Jr., & Fabricant, D. G. 1981, IEEE Trans. Nucl. Sci., NS-28, 869

Grillo, F., Sciortino, S., Micela, G., Vaiana, G.S., & Harnden, F.R., Jr. 1992, ApJS, 81, 795

Hambly, N.C., Hawkins, M.R.S., & Jameson, R.F. 1993, A&AS, 100, 607

Harnden, F.R., Jr., Fabricant, D.G., Harris, D.E., & Schwarz, J. 1984, SAO Special Report, 393

Hasinger, G., Boesse, G., Predehl, P., Turner, J., Yusaf, R., George, I.M., & Rohrbach, G. 1993, MPE/OGIP Calibration Memo CAL/ROS/93-015, in Legacy 9

Hertzsprung, E. 1947, Ann. Leiden Obs., 19, Part 1A

Hodgkin, S. T., Jamenson, R. F., & Steele, I. A. 1995, MNRAS, in press.

Kashyap, V., Micela, G., Sciortino, S., Harnden, F.R., Jr., & Rosner, R. 1994, in The Soft X-ray Cosmos, ed. E. M. Schlegel & R. Petre, (AIP Conference Proceedings 313), p. 239.

Kato, T., 1976, ApJS, 30, 397

Maggio, A., Sciortino, S., Vaiana, G.S., Majer, P., Bookbinder, J., Golub, L., Harnden, F.R., Jr., & Rosner, R. 1987, ApJ, 315, 687

Mason, B.D., Hartkopf, W.I., & McAlister, H.A. 1993, AJ, 106, 637

Mermilliod, J.-C., Rosvick, J.M., Duquennoy, A., & Mayor, M. 1992, A&A, 265, 513

Micela, G. 1991, PhD Thesis, Universitá di Palermo

Micela, G., Sciortino, S., Serio, S., Vaiana, G.S., Bookbinder, J., Golub, L., Harnden, F.R., Jr., & Rosner, R. 1985, ApJ, 292, 172

Micela, G., Sciortino, S., Vaiana, G.S., Schmitt, J.H.M.M., Stern, R.A., Harnden, F.R., Jr., & Rosner, R. 1988, ApJ, 325, 798

Micela, G., Sciortino, S., Vaiana, G.S., Schmitt, J.H.M.M., Harnden, F.R., Jr., & Rosner, R. 1990, ApJ, 348, 557 (Paper I)
Mihalas, D. 1978, Stellar Atmospheres, 2nd ed. (San Francisco: W.H. Freeman), p. 185
Nousek, J. A., & Lesser, A. 1993, Rosat Newsletter, 8, 13
Pallavicini, R., Golub, L., Rosner, R., Vaiana, G.S., Ayres, T., & Linsky, J.L. 1981, ApJ, 248, 279
Patten, B. M., & Simon, T. 1993, ApJ, 415, L23
Pye, J. P., Hodgkin, S. T., Stern, R. A., & Stauffer, J. R. 1994, MNRAS, 266, 798.
Randich, S., & Schmitt, J.H.M.M. 1994, A&A, in press.
Rosner, R., Golub, L., & Vaiana, G.S. 1985, ARA&A, 23, 413
Rosvick, J. M., Mermilliod, J.-C., & Mayor, M. 1992, A&A, 255, 130.
Schachter, J., Remillord, R., Saar, S., Favata, F., Sciortino, S., & Barbera, M. 1994, ApJ, submitted
Schmitt, J.H.M.M. 1985, ApJ, 293, 178
Schmitt, J.H.M.M., Golub, L., Harnden, F.R., Jr., Maxson, C.W., Rosner, R., & Vaiana, G.S. 1985, ApJ, 290, 307
Schmitt, J.H.M.M., Kahabka, P., Stauffer, J., & Peiters, A. 1993, A&A, 277, 114
Schmitt, J.H.M.M., Micela, G., Sciortino, S., Vaiana, G.S., Harnden, F.R., Jr., & Rosner, R. 1990, ApJ, 351, 492
Sciortino, S., & Micela, G. 1992, ApJ, 388, 595
Sciortino, S., Micela, G., Kashyap, V., Harnden, F.R., Jr., & Rosner, R. 1994, in Cool Stars, Stellar Systems, and The Sun - Eight Cambridge Workshop, ed. J.-P. Caillault, (San Francisco: A.S.P. Conference Series), 140.
Snowden, S.L., McCammon, D., Burrows, D.N., & Mendenhall, J.A. 1994, ApJ, 424, 714
Soderblom, D.R., et al. 1993, ApJS, 85, 315
Stauffer, J., & Hartmann, L., 1987, ApJ, 318, 337
Stauffer, J., Klemola, A., Prosser, C., & Probst, R. 1991, AJ, 101, 980
Stauffer, J., R., Caillault, J.-P., Gagne, M., Prosser, C.F., & Hartmann, L.W. 1994, ApJS, 91, 625
Stern, R.A., Zolcinsky, M.C., Antiochos, S.C., & Underwood, J.M. 1981, ApJ, 249, 647
Stern, R.A., Schmitt, J. H. M. M., Rosso, C., Pye, J., Hodgkin, S. T., & Stauffer, J. R. 1992, ApJ, 399, L159
Stern, R.A., Schmitt, J. H. M. M., Rosso, C., Pye, J., Hodgkin, S. T., & Simon, T. 1994, ApJ, 427, 808
Strom, K.M. 1990, ApJ, 362, 168
Vaiana, G.S., Maggio, A., Micela, G., & Sciortino, S. 1992, Mem. SAIt., 63, 545

Vilhu, O. 1984, A&A, 133, 117

Vilhu, O., & Walter, F. 1987, ApJ, 321, 958.

Walter, F.W. 1982, ApJ, 253, 745

Worrall, D. M., et al. 1992, in 'Data Analysis in Astronomy IV', ed. V. di Gesù et al., (New York: Plenum), 145.

Zimmermann, H. U., Belloni, T., Izzo, C., Kahabka, P., & Schwentker, O. 1993, EXSAS User's Guide (Third Edition), MPE Report, 244, ISSN 0178-0719

Table 1: Pleiades Stars in Our Observation

#	Name	RA(h:m:s)$_{J2000}$	Dec(∘ ' ")$_{J2000}$	V	Ref.	B-V	SP	Ref.	Vsini	Notes	Ref.
1	Hz81	3:43:19.1	23:51:39.2	13.55	1	0.92	G8V	2	...	...	
2	Hz83	3:43:19.6	23:51:01.2	14.86	1	1.05	K0V	2	...	...	
3	Hz120	3:43:31.9	23:40:30.4	10.79	3	0.70	G1	4	11	...	
4	Hz129	3:43:34.3	23:45:46.3	11.47	3	0.88	G8	4	<7	var, bin	5, 6
5	Hz134/T68/MT40	3:43:36.6	24:13:57.2	14.41	1	1.51	K7Ve	2	40	...	
6	Hz152	3:43:37.7	23:32:13.1	10.75	3	0.70	G1	4	<7	...	
7	HCG124	3:43:39.0	23:44:07.0	18.05	7	...	...		...	...	
8	Hz157	3:43:41.4	23:39:01.9	7.90	3	0.34	A9V	8	100	bin?	5
9	Hz164	3:43:42.7	23:35:43.8	9.54	3	0.48	F5V	8	30	...	
10	Hz189	3:43:48.5	23:32:25.5	14.00	9	1.37	K5.5Ve	2	<10	var	10
11	Hz193	3:43:50.7	24:14:55.3	11.29	3	0.81	...		9	...	
12	Hz220	3:43:55.5	23:41:16.0	...		...	...		...	...	
13	HCG133	3:43:57.3	24:13:21.9	17.57	7	...	...		...	...	
14	JRS27/B477	3:43:57.0	23:57:07.9	17.93	9	1.06	...		...	...	
15	Hz233	3:43:58.8	23:53:02.8	9.66	3	0.52	F6V	8	13	...	
16	Hz248	3:44:00.5	23:32:41.7	11.02	3	0.77	G1	4	12	bin	6
17	JRS26	3:44:01.7	23:51:47.6	17.22	9	1.95	...		...	...	
18	Hz263	3:44:04.7	24:16:35.5	11.54	3	0.88	G8	4	10	...	
19	Hz296	3:44:11.1	23:22:49.1	11.36	9	0.83	G8	4	15	var, bin	5, 6
20	Hz298	3:44:12.7	24:01:59.0	10.86	3	0.88	...		8	bin?	5
21	Hz299	3:44:13.0	24:01:55.0	10.86	3	0.88	...		...	bin?	5
22	Hz303	3:44:14.5	24:06:11.9	10.48	3	0.88	...		15	bin?	5
23	HCG144	3:44:16.4	23:37:05.8	17.69	7	...	...		...	...	
24	HCG145	3:44:17.7	24:26:48.7	16.51	7	...	...		...	...	
25	HCG155	3:44:20.8	23:33:41.5	17.42	7	...	...		...	...	
26	Hz335/T73/MT53	3:44:23.0	24:04:07.4	13.76	1	1.28	K5Ve	2	73	var	10
27	Hz338	3:44:23.5	24:08:01.4	9.07	3	0.46	F2V	11	<40	...	
28	Hz344	3:44:25.6	24:23:45.2	8.17	3	0.27	A8-K7e	8	200	...	
29	HCG156	3:44:26.8	24:24:33.2	16.07	7	...	...		...	...	
30	Hz357/T8/MT54	3:44:27.9	24:10:19.1	13.34	9	1.22	M0.5-K	9,12	<10	var	10
31	Hz370	3:44:31.9	23:52:35.8	14.56	3	1.18	...		...	...	
32	Hz390	3:44:35.4	24:00:08.6	14.40	3	1.16	...		...	...	
33	A23/A57/A86/B139	3:44:36.3	23:30:12.5	16.55	9	1.57	...		...	...	
34	Hz430	3:44:43.8	24:13:56.1	11.37	9	0.82	G8	4	<7	...	
35	Hz447	3:44:48.1	24:17:26.9	5.46	3	-0.04	B7IV	8	260	16Tau, Celaeno	
36	Hz470	3:44:51.1	23:16:10.6	8.95	3	0.39	F3V	8	<40	...	
37	Hz468	3:44:52.4	24:06:51.6	3.71	3	-0.11	B6III	8	220	SB1, 17Tau, Electra	13
38	Hz476	3:44:53.8	23:55:20.5	10.78	9	0.80	F9V	11	23	bin?	5
39	Hz489	3:44:56.4	24:26:01.4	10.39	3	0.63	G0V	8	17	...	
40	Hz513	3:44:58.9	23:23:24.2	13.84	1	1.31	K7Ve	2	...	...	

Table 1: Continued

#	Name	RA(h:m:s)$_{J2000}$	Dec(° ' ")$_{J2000}$	V	Ref.	B-V	SP	Ref.	Vsini	Notes	Ref.
41	Hz522	3:45:03.2	23:50:26.9	11.97	9	0.90	K2V	11	<7	bin	6
42	Hz530	3:45:05.2	23:42:13.8	8.95	3	0.39	F2V	8	<12	...	
43	Hz531	3:45:06.5	24:15:52.8	8.58	3	0.34	Am?	8	75	...	
44	Hz554	3:45:11.9	24:35:14.4	14.09	3	0.92	K5Ve	2	...	...	
45	Hz563	3:45:12.3	24:28:06.4	4.31	3	-0.11	B6V	8	135	SB1, 19Tau, Taygeta	13
46	HCG185	3:45:12.1	23:21:54.4	17.64	7	...	...		...	...	
47	A84/B196	3:45:16.6	24:34:34.2	16.18	9	1.57	...		...	...	
48	HCG183	3:45:16.1	24:07:17.2	14.91	7	...	...		...	...	
49	Hz625	3:45:21.1	23:43:43.9	12.57	3	1.10	K0V	11	94	bin?, var	5
50	Hz636	3:45:22.1	23:28:22.8	12.48	3	1.06	...		<7	...	
51	Hz652	3:45:26.1	24:02:10.6	8.04	3	0.21	A3V	8	235	...	
52	SK520	3:45:27.7	23:10:14.4	16.88	7	...	...		...	...	
53	Hz676/T162	3:45:29.5	23:45:39.4	13.64	9	1.30	K3.5Ve	2	<10	...	
54	Hz673/MT59	3:45:30.2	24:18:49.3	15.46	3	1.47	dK7e	12	...	...	
55	Hz686/MT59a/T13	3:45:32.9	24:18:13.2	13.38	10	1.27	K7Ve	12	64	var	5
56	Hz697	3:45:34.4	24:27:52.1	8.60	3	0.35	A9V	8	75	var	11
57	Hz708	3:45:35.3	24:05:04.0	10.13	3	0.62	F9V	8	46	...	
58	B203	3:45:36.8	24:39:08.0	16.70	14	...	...		...	...	
59	Hz717	3:45:37.7	24:20:12.9	7.18	3	0.16	A1V	8	15	bin, Vel var?	
60	Hz727	3:45:40.2	24:37:42.7	9.70	3	0.55	F9V	8	50	var	5
61	Hz738	3:45:39.3	23:45:19.8	12.26	3	1.16	G9V	11	50	bin?, var	5
62	Hz745	3:45:41.4	24:17:22.7	9.45	3	0.52	F5V	8	65	...	
63	Hz746	3:45:41.7	24:25:57.6	11.27	3	0.92	G5	4	<7	var	5
64	Hz762/T63b	3:45:43.9	24:04:30.5	14.33	1	1.42	...		<10	...	
65	Hz761	3:45:44.3	24:13:17.5	10.55	3	0.67	G2V	11	11	bin	6
66	Hz793/T46	3:45:48.9	23:51:11.2	14.31	9	1.47	M0-1V	12	<10	...	
67	Hz785	3:45:49.6	24:22:08.2	3.88	3	-0.07	B7III	8	40	bin?, 20Tau, Maia	13
68	Hz801	3:45:48.9	23:08:54.2	6.85	3	0.04	A0V	8	190	SB2	13
69	Hz799	3:45:50.4	23:52:31.1	13.70	9	1.34	K5V	11	<10	flare?	10
70	Hz804	3:45:51.6	24:02:24.1	7.85	3	0.20	A2V	8	170	...	
71	Hz813	3:45:53.7	24:28:13.9	15.30	3	1.18	M1-2	15	...	...	
72	Hz817	3:45:54.4	24:33:20.9	5.76	3	-0.04	B8V	8	220	21Tau, Asterope	
73	Hz859	3:46:02.9	24:31:44.4	6.43	3	-0.02	B9V	8	250	22Tau	
74	Hz870	3:46:02.8	23:44:18.3	12.68	5	1.26	G4.5V	11	9	bin?	5
75	Hz882	3:46:04.1	23:24:24.3	12.66	3	1.07	K3V	11	65	var	5
76	SK488	3:46:05.6	24:36:46.2	15.81	16	...	M2.8	16	...	...	
77	Hz879	3:46:06.4	24:34:07.1	12.82	1	1.08	...		<7	var	5
78	Hz883/T70b	3:46:06.9	24:33:47.1	13.05	1	1.15	...		<7	var?	5
79	Hz890/A121	3:46:07.4	24:22:32.1	14.80	3	1.33	M0Ve	2	<10	...	
80	Hz915/T71b/MT67	3:46:08.2	23:20:55.0	13.62	3	1.23	K6Ve	2	12	...	

Table 1: Continued

#	Name	RA(h:m:s)$_{J2000}$	Dec(° ' ")$_{J2000}$	V	Ref.	B-V	SP	Ref.	Vsini	Notes	Ref.
81	Hz906/T14/MT65	3:46:09.9	24:40:26.0	15.20	3	1.52	dM2e	12	...	bin?	9
82	Hz923	3:46:09.9	23:20:28.9	10.12	3	0.62	G1V	4	18	var	5
83	Hz916	3:46:11.7	24:37:24.8	11.71	3	0.87	G8V	4	<7	...	
84	Hz930/VM2	3:46:12.7	24:03:20.8	14.23	1	1.34	...		15	...	
85	Hz948	3:46:12.7	23:07:46.7	8.66	3	0.60	G0V	8	< 7	...	
86	Hz956	3:46:15.9	24:11:27.6	7.96	3	0.32	A7V	8	150	bin?	5
87	Hz975	3:46:17.9	23:29:15.4	10.58	9	0.84	G0	4	...	bin?	5
88	Hz980	3:46:19.4	23:56:58.3	4.18	3	-0.06	B6IVn	8	275	bin, 23Tau, Merope	17
89	Hz996	3:46:22.5	24:34:17.2	10.42	3	0.64	G0V	8	10	var?	5
90	VM6/A2/A76/T46	3:46:25.4	24:09:38.0	15.77	3	1.32	...		...	bin?	9
91	Hz1028	3:46:27.2	24:15:22.9	7.35	3	0.10	A2V	8	110	...	
92	Hz1032/VM8	3:46:28.3	24:26:06.8	11.1	9	0.75	G8	4	36	var	5
93	Hz1039/A148	3:46:27.7	23:35:34.8	13.07	10	1.23	K2V	10	<7	var, bin	5,9
94	Hz1061/T48/VM9	3:46:31.1	24:07:03.6	14.23	9	1.39	K5V	18	<10	...	
95	Hz1081	3:46:32.8	23:18:23.5	14.61	9	1.42	K7Ve	2	<10	...	
96	Hz1084	3:46:34.2	23:37:30.5	8.11	3	0.36	A0V	8	150	...	
97	Hz1094/K3/T195	3:46:35.9	23:58:05.3	14.02	3	1.40	...		...	...	
98	Hz1103/T151	3:46:35.3	23:24:43.4	14.77	9	1.48	K7Ve	2	...	...	
99	Hz1100/T143b/VM11	3:46:37.3	24:20:38.3	12.25	9	1.10	K3V	18	<10	bin?	9
100	SK465	3:46:36.0	23:04:18.3	17.70	7	...	...		...	...	
101	Hz1117	3:46:37.7	23:47:20.2	10.22	11	0.71	G6V	11	<7	bin?	5
102	Hz1110/VM12	3:46:38.8	24:31:17.2	13.41	10	1.23	K6.5Ve	2	<7	...	
103	Hz1122	3:46:39.2	24:06:16.2	9.29	3	0.46	F4V	8	28	...	
104	Hz1124/VM14	3:46:39.2	24:01:51.2	12.12	3	0.92	K2V	11	7.5	var, bin	5, 6
105	Hz1136	3:46:40.1	23:29:56.1	12.02	3	0.99	G8V	11	80	var, bin?	5,9
106	Hz1139	3:46:40.0	23:06:41.1	9.38	3	0.48	F5V	8	33	...	
107	VM15	3:46:43.3	23:59:42.9	16.07	3	0.99	...		...	...	
108	Hz1173/T81/MT70	3:46:49.2	24:36:01.6	15.10	9	1.56	dM2	9	<10	...	
109	SK459	3:46:48.3	23:04:41.6	14.29	7	...	...		...	...	
110	HCG245	3:46:48.7	23:04:08.5	16.04	7	...	...		...	...	
111	Hz1200	3:46:50.5	23:14:24.4	9.90	3	0.54	F6V	19	<20	...	
112	MT72/VM16/T15	3:46:53.6	24:17:16.3	16.09	3	1.12	dM1-2e	12	...	var	12
113	Hz1215	3:46:53.6	23:35:05.3	10.52	3	0.65	G0V	8	<7	...	
114	A40	3:46:57.1	23:15:03.0	15.50	14	...	...		...	...	
115	Hz1234	3:46:59.2	24:31:16.9	6.82	3	0.02	B9.5V	12	260	...	
116	Hz1275	3:47:01.3	23:29:45.8	11.45	9	0.83	K0V	11	7	...	
117	Hz1280/T27b/VM19	3:47:03.5	24:09:35.7	14.55	1	1.37	dK7,M0	18	...	...	
118	Hz1284	3:47:04.1	23:59:46.6	8.37	3	0.30	A9V	8	100	...	
119	Hz1286/T16	3:47:03.8	23:36:59.6	15.34	9	1.68	dM2.5	9	...	bin?	9
120	Hz1298	3:47:06.7	23:42:58.5	12.18	3	1.02	...		<7	...	

Table 1: Continued

#	Name	RA(h:m:s)$_{J2000}$	Dec(o ' ")$_{J2000}$	V	Ref.	B-V	SP	Ref.	Vsini	Notes	Ref.
121	HCG253	3:47:08.1	24:18:26.4	16.00	7	...	...		...	...	
122	Hz1305/B358	3:47:07.3	23:13:36.4	13.55	9	1.20	...		84	...	
123	Hz1306/T17	3:47:08.5	23:42:40.4	13.45	9	1.31	K5Ve	18	15	flare	3
124	Hz1321/T28b	3:47:09.3	23:44:36.3	15.22	9	1.47	dM3	9	17	bin?	9
125	Hz1309	3:47:010.0	24:16:40.3	9.46	3	0.47	F6V	8	85	...	
126	Hz1332	3:47:13.4	23:42:56.0	12.53	9	1.02	K4V	11	7.5	var	5
127	B363	3:47:13.6	23:49:55.1	15.78	9	1.35	...		...	...	
128	Hz1338	3:47:16.5	24:07:45.9	8.69	3	0.46	F3V	8	10	bin?	5
129	Hz1348/VM24	3:47:17.9	24:23:31.8	12.75	9	1.15	K5	18	<10	bin?	9
130	Hz1355/T45b	3:47:18.1	24:02:12.8	14.07	9	1.4	dM1.5	9	<10	bin?	9
131	Hz1362	3:47:19.2	24:08:25.7	8.25	3	0.26	A7V	8	<12	var	11
132	Hz1375	3:47:21.0	24:07:02.6	6.29	3	0.02	A0V	8	160	bin?	13
133	Hz1380	3:47:20.8	23:48:15.6	6.99	3	0.03	A1V	8	235	...	
134	HCG266	3:47:22.6	23:44:08.5	17.50	7	...	...		...	...	
135	Hz1384	3:47:23.9	24:35:22.5	7.66	3	0.21	A4V	8	215	...	
136	Hz1392	3:47:23.9	23:54:56.4	10.36	20	...	F9V	19	<20	...	
137	Hz1397	3:47:24.4	23:54:56.4	7.26	3	0.05	A2V+G5V	8,20	<10	bin, Vel var?	5
138	HCG270	3:47:23.8	23:08:58.4	17.34	7	...	...		...	...	
139	Hz1425	3:47:26.7	23:40:46.2	7.77	3	0.15	A3V	8	185	var	11
140	SK417	3:47:28.0	23:26:55.2	17.11	7	...	...		...	...	
141	Hz1432	3:47:29.0	24:06:22.1	2.87	3	-0.09	B7III	8	220	ηTau, Alcyone	
142	Hz1431	3:47:29.4	24:17:22.1	6.81	3	0.06	A0V	8	40	SB2	13
143	HCG273	3:47:30.6	24:22:14.0	15.59	7	...	...		...	...	
144	Hz1454/T57b	3:47:33.6	24:41:06.9	12.87	10	1.12	K3V	10	<10	...	
145	MT78/T105	3:47:33.4	23:41:33.9	15.73	9	1.45	dM3e	8	...	bin?	9
146	Hz1512	3:47:38.0	23:28:08.6	13.50	3	1.37	K6	18	<10	var	5
147	Hz1516/T64b/MT80	3:47:40.2	24:18:10.5	13.97	9	1.34	...		...	...	
148	Hz1514	3:47:40.3	24:21:56.4	10.48	3	0.64	G5	21	15	...	
149	Hz1532/B270	3:47:41.2	23:44:26.4	13.90	1	1.29	...		50	...	
150	Hz1531/T19/VM35	3:47:41.4	23:58:20.4	13.41	10	1.22	dK7,dM0	12	50	var	5
151	ALR513	3:47:46.6	24:02:50.1	11.11	22	1.23	...		...	...	
152	Hz1593	3:47:48.0	23:13:09.0	11.11	1	0.86	G6V	11	<7	...	
153	HCG295	3:47:50.9	24:30:19.8	14.87	7	...	...		...	...	
154	A60/B240	3:47:50.9	24:30:19.8	16.10	14	...	...		...	...	
155	ALR929	3:47:51.8	24:30:23.8	16.16	9	1.56	...		...	...	
156	Hz1613	3:47:52.4	23:56:32.7	9.88	3	0.54	F8V	8	19	var?	5
157	HCG302	3:47:55.2	23:19:07.5	17.33	7	...	...		...	...	
158	ALR928	3:47:57.0	24:31:43.5	13.77	1	1.03	...		...	...	
159	Hz1695/VM38	3:48:04.1	24:04:02.0	15.45	3	1.43	...		...	...	
160	SK384	3:48:05.7	23:16:11.9	16.07	7	...	...		...	...	

Table 1: Continued

#	Name	RA(h:m:s)$_{J2000}$	Dec(∘ ' ")$_{J2000}$	V	Ref.	B-V	SP	Ref.	Vsini	Notes	Ref.
161	Hz1726	3:48:07.1	24:08:35.8	9.25	3	0.55	F7V	11	12	bin?, var?	5
162	Hz1756	3:48:10.9	23:30:28.6	14.11	1	1.37	...		<10	...	
163	Hz1762	3:48:13.5	24:19:10.4	8.27	3	0.36	A9V	8	180	...	
164	HCG315	3:48:13.7	23:38:00.4	17.72	7	...	...		...	...	
165	Hz1785/T84/VM41	3:48:17.3	24:30:17.2	14.29	1	1.40	...		<10	...	
166	Hz1797	3:48:16.8	23:38:16.2	10.11	3	0.56	F9V	8	21	var	5
167	Hz1794/VM42	3:48:17.1	23:53:29.2	13.36	3	0.64	...		12	...	
168	Hz1805/VM43	3:48:17.9	23:53:33.1	13.36	3	0.64	...		...	...	
169	Hz1823	3:48:20.8	23:25:21.0	5.45	3	-0.07	B8V	8	270	...	
170	Hz1827/T51	3:48:22.8	23:58:22.9	14.87	9	1.47	...		...	bin?	9
171	Hz1856	3:48:26.1	24:02:58.7	10.02	3	0.56	F8V	8	16	...	
172	HCG332	3:48:26.5	23:11:31.6	17.87	7	...	...		...	...	
173	Hz1883/T48b	3:48:28.0	23:18:03.5	12.64	10	1.07	K2V	10	140	var, bin	5, 6
174	Hz1876	3:48:29.9	24:20:47.4	6.95	3	0.12	A1V	8	105	bin?	5
175	VM46/T156	3:48:31.3	24:16:29.3	16.01	9	1.59	dM3	9	...	...	
176	Hz1912	3:48:34.8	24:10:56.1	9.05	3	0.49	F4V	8	75	bin?	5
177	Hz1924	3:48:34.4	23:26:09.2	10.33	3	0.62	G0V	8	13	var?	5
178	HCG337	3:48:39.9	24:12:42.8	16.68	16	...	...		...	...	
179	Hz1993	3:48:43.7	23:15:39.6	8.37	3	0.29	A8V	8	85	...	
180	Hz2016/MT95/T72b	3:48:45.3	23:20:23.5	13.61	9	1.22	dK7	12	11	...	
181	Hz2027	3:48:48.9	24:16:06.3	10.91	3	0.86	K0	21	<8	bin?, var	5
182	Hz2034/T9b/VM49	3:48:49.3	23:58:39.2	12.51	10	1.04	K2.5V	10	75	var	5
183	ALR728	3:48:51.1	24:12:02.2	16.09	9	1.46	...		...	...	
184	Hz2126	3:49:02.2	23:15:12.4	11.64	3	0.86	K0	4	<7	var?	5
185	ALR715	3:49:03.7	24:18:50.4	15.08	1	0.95	...		...	...	
186	HCG354	3:49:05.8	23:44:24.2	15.31	7	...	...		...	...	
187	Hz2144/T157	3:49:05.9	23:44:24.2	15.31	9	1.45	...		...	bin?	9
188	Hz2147	3:49:05.9	23:46:56.2	10.83	3	0.80	K0V	11	27	bin?, var	5
189	ALR1381	3:49:06.0	23:44:28.2	15.34	1	1.54	...		...	...	
190	Hz2168	3:49:09.7	24:03:17.0	3.64	3	-0.08	B8III	8	215	SB1, 27Tau, Atlas	13
191	Hz2181	3:49:11.0	24:08:16.9	5.09	3	-0.08	B8p	8	340	var, 28Tau, Pleione	11
192	Hz2193/T88	3:49:11.3	23:33:19.9	14.1810		1.47	K6Ve	2	23	...	
193	Hz2195	3:49:12.2	23:53:16.8	8.12	3	0.22	A7V	8	160	...	
194	Hz2208/T107/A139	3:49:15.3	24:30:03.7	14.46	9	1.36	K6Ve	2	73	...	
195	Hz2220	3:49:16.8	24:23:50.6	7.52	3	0.10	A2V	8	240	...	
196	HCG362	3:49:16.4	24:03:50.6	15.00	7	...	...		...	...	
197	Hz2263	3:49:21.6	24:22:55.3	6.60	3	-0.03	B9.7V	8	90	...	
198	HCG363	3:49:21.5	23:39:08.3	17.15	7	...	...		...	...	
199	Hz2284/VM57	3:49:23.9	23:50:25.1	11.35	3	0.78	...		<7	var	5
200	Hz2289	3:49:25.9	24:14:56.0	7.97	3	0.18	A3V	8	165	var?	5

Table 1: Continued

#	Name	RA(h:m:s)$_{J2000}$	Dec(o ' ")$_{J2000}$	V	Ref.	B-V	SP	Ref.	Vsini	Notes	Ref.
201	Hz2311/VM59	3:49:28.7	23:42:48.8	11.35	9	0.82	...		8	var	5
202	Hz2345	3:49:32.5	23:22:53.6	9.10	3	0.44	F3V	8	130	...	
203	Hz2341	3:49:33.1	23:47:46.6	10.87	3	0.71	G4V	11	<7	bin	6
204	Hz2368/K23	3:49:34.9	23:27:18.4	14.02	10	1.34	...		...	...	
205	Hz2366/VM61	3:49:36.5	24:17:49.4	11.53	3	0.82	...		<7	...	
206	Hz2425	3:49:43.5	23:42:46.9	6.17	3	-0.05	B9V	8	310	...	
207	Hz2462/VM64	3:49:50.3	23:42:23.5	11.49	9	0.84	...		<7	...	
208	Hz2500	3:49:57.3	23:50:56.1	10.95	20	...	F9.5V	20	...	...	
209	Hz2503	3:49:57.8	23:50:57.1	...		...	...		...	...	
210	Hz2507	3:49:58.0	23:50:59.0	6.74	3	0.06	A0V	8	15	bin	5
211	SK293	3:49:58.3	23:42:35.0	15.92	16	...	M2.6	16	...	...	
212	Hz2548/VM69	3:50:05.0	24:07:30.6	14.02	9	1.33	K5.5Ve	2	<10	...	
213	T28	3:50:11.2	23:55:42.2	16.50	14	...	...		...	...	
214	Hz2602/T93	3:50:12.3	23:59:46.2	15.49	9	1.63	dM3	9	<15	bin?	9

All rotational velocities are from Soderblom et al. 1993

References

1 - Landolt 1979
2 - Kraft & Greenstein 1969
3 - Johnson & Mitchell 1958
4 - Wilson 1963
5 - Van Leeuwen 1983; van Leeuwen and Alphenaar 1982
6 - Soderblom 1993
7 - Stauffer et al. 1991
8 - Mendoza 1956, 1967
9 - Stauffer 1980, 1982, 1984; Stauffer et al. 1984
10 - Iriarte 1967
11 - Breger 1972
12 - McCarthy 1969
13 - Abt 1965
14 - Jones 1970, 1973, 1981
15 - Pesch 1962
16 - Prosser, Stauffer & Kraft 1991
17 - Hoffleit & Jaschek 1982
18 - Herbig 1962
19 - Kraft 1967
20 - Buscombe 1977, 1980, 1981
21 - Danzinger & Conti 1966
22 - Ahmed, Lawrence & Reddish 1965

Table 5: X-Ray Luminosity of Pleiades Stars

#	Name	$\Delta R.A.$ ["]	$\Delta Dec.$ ["]	Off-axis [']	CtRt	S/N	HR	$cecf$	$\log(L_x)$	Multiple Counterparts
(1)		(2)	(2)		(3)			(4)	(5)	(6)
1*	Hz81	...	...	47.8	<7.50	...	...	1.88	<29.44	
2*	Hz83	...	...	47.7	<7.39	...	...	2.31	<29.52	
3	Hz120	...	...	46.9	<7.68	...	...	1.21	<29.26	
4*	Hz129	...	...	45.1	<7.33	...	...	1.21	<29.24	
5*	Hz134/T68/MT40	...	...	48.0	<8.79	...	...	1.88	<29.50	
6	Hz152	...	...	48.7	<8.72	...	...	1.21	<29.31	
7	HCG124	...	...	44.4	<12.02	...	...	1.21	<29.45	
8	Hz157	...	...	45.3	<8.06	...	...	1.21	<29.28	
9	Hz164	16.0	-22.1	46.2	21.23	7.70	1.11 ± 0.26	1.15	29.67	
10*	Hz189	...	...	46.4	<8.39	...	...	2.31	<29.57	
11	Hz193	...	...	45.6	8.13	6.13	0.88 ± 0.28	1.12	29.25	1
12	Hz220	...	...	41.5	<6.33	...	...	1.21	<29.17	
13	HCG133	...	...	43.5	8.13	6.13	0.88 ± 0.28	1.12	29.25	1
14	JRS27/B477	...	...	39.2	<5.94	...	...	1.21	<29.14	
15	Hz233	...	...	38.7	<5.29	...	...	1.21	<29.09	
16	Hz248	...	...	43.9	<8.32	...	...	1.21	<29.29	
17	JRS26	...	...	38.1	<5.71	...	...	1.21	<29.13	
18	Hz263	...	...	43.6	<15.39	...	...	1.21	<29.56	
19	Hz296	15.5	6.1	47.6	33.99	11.12	1.73 ± 0.27	1.29	29.93	
20	Hz298	...	...	36.4	48.69	21.92	...	1.21	29.76	2
21	Hz299	...	...	36.3	48.69	21.92	...	1.21	29.76	2
22	Hz303	...	...	37.1	61.39	22.57	...	1.21	29.86	2
23	HCG144	6.4	-3.4	38.6	29.97	12.13	1.02 ± 0.16	1.14	29.82	
24	HCG145	...	...	47.5	<9.86	...	...	1.21	<29.36	
25	HCG155	...	...	39.3	<7.56	...	...	1.21	<29.25	
26	Hz335/T73/MT53	...	...	34.6	10.15	5.93	...	1.21	29.08	2
27	Hz338	...	...	35.9	25.5	10.61	...	1.21	29.48	2
28	Hz344	...	...	44.1	<7.71	...	...	1.21	<29.26	
29	HCG156	...	...	44.4	<7.78	...	...	1.21	<29.26	
30	Hz357/T8/MT54	...	...	35.9	16.13	8.57	...	1.21	29.28	2
31	Hz370	...	...	31.1	<4.55	1.89	...	1.21	<29.03	
32	Hz390	...	...	30.9	<4.64	...	...	1.21	<29.04	
33	A23/A57/A86/B139	...	...	38.4	<5.44	...	...	1.21	<29.11	
34	Hz430	...	...	34.7	<5.27	...	...	1.21	<29.09	
35	Hz447	...	...	36.0	<6.12	...	...	1.21	<29.16	
36	Hz470	...	...	46.3	<6.94	...	...	1.21	<29.21	
37	Hz468	...	...	29.4	<3.92	...	...	1.21	<28.96	
38	Hz476	17.2	10.5	26.1	10.31	6.59	1.71 ± 0.51	1.28	29.41	
39	Hz489	...	...	40.9	<7.14	...	...	1.21	<29.22	
40	Hz513	-21.4	85.4	39.5	7.82	3.90	1.92 ± 0.87	1.34	29.31	
41	Hz522	...	...	24.2	5.10	4.04	8.09 ± 6.89	1.93	29.28	
42	Hz530	...	...	26.3	<3.79	...	...	1.21	<28.95	
43	Hz531	...	...	31.9	<4.16	...	...	1.21	<28.99	
44	Hz554	...	...	46.7	<8.72	...	...	1.21	<29.31	
45	Hz563	20.2	-10.7	40.5	33.63	11.73	1.53 ± 0.23	1.24	29.91	
46	HCG185	...	...	38.9	<7.04	...	...	1.21	<29.22	

Table 5: Continued

#	Name	$\Delta R.A.$ ["]	$\Delta Dec.$ ["]	Off-axis [']	CtRt	S/N	HR	$cecf$	$\log(L_x)$	Multiple Counterparts
(1)		(2)	(2)		(3)			(4)	(5)	(6)
47	A84/B196	...	...	45.6	<9.11	...	...	1.21	<29.33	
48	HCG183	...	...	24.8	<5.91	...	...	1.21	<29.14	
49*	Hz625	-7.5	-0.4	22.4	35.05	12.91	0.58 ± 0.09	1.96	30.12	
50	Hz636	8.6	-116.2	32.3	9.26	4.19	0.83 ± 0.42	1.13	29.31	
51	Hz652	...	...	20.4	<4.64	...	...	1.21	<29.04	
52	SK520	...	...	47.5	<8.25	...	...	1.21	<29.29	
53*	Hz676/T162	...	...	19.8	<4.31	...	...	2.31	<29.28	
54	Hz673/MT59	...	...	30.5	24.89	15.53	...	1.21	29.47	3
55	Hz686/MT59a/T13	...	...	29.7	25.78	15.53	...	1.21	29.48	3
56	Hz697	...	...	37.8	<7.23	...	...	1.21	<29.23	
57	Hz708	8.7	3.5	20.0	23.82	7.95	0.94 ± 0.25	1.13	29.72	
58	B203	...	...	48.0	31.86	9.62	1.97 ± 0.37	1.35	<29.92	
59	Hz717	...	...	30.7	5.36	4.30	...	1.21	28.80	3
60	Hz727	5.4	-12.5	46.4	31.86	9.62	1.97 ± 0.37	1.35	29.92	
61*	Hz738	-0.2	2.3	17.9	43.41	16.87	0.69 ± 0.08	1.99	30.22	
62	Hz745	...	...	27.9	13.61	10.81	...	1.21	29.20	3
63	Hz746	64.6	-17.8	35.4	7.67	4.24	1.04 ± 0.51	1.14	29.23	
64	Hz762/T63b	...	...	18.0	4.45	3.31	0.94 ± 0.60	1.13	28.99	
65	Hz761	3.0	3.8	47.8	24.25	15.99	2.01 ± 0.23	1.36	30.02	
66	Hz793/T46	...	...	13.8	2.33	3.46	1.84 ± 0.98	1.32	28.77	
67	Hz785	...	...	31.1	<5.10	...	...	1.21	<29.08	
68	Hz801	...	...	47.1	<7.49	...	...	1.21	<29.24	
69*	Hz799	4.2	-2.7	13.3	3.35	4.16	1.01 ± 0.57	2.31	29.18	
70	Hz804	...	...	15.4	<2.31	...	...	1.21	<28.73	
71	Hz813	...	...	36.4	<6.10	...	...	1.21	<29.16	
72	Hz817	...	...	41.2	<7.56	...	...	1.21	<29.25	
73	Hz859	...	...	39.1	<9.89	...	...	1.21	<29.37	
74*	Hz870	-2.8	2.8	14.2	4.31	4.84	0.66 ± 0.31	1.98	29.22	
75	Hz882	-33.7	9.1	31.3	19.93	8.55	0.83 ± 0.19	1.13	29.64	
76	SK488	...	...	43.9	<14.40	...	...	1.21	<29.53	
77	Hz879	...	...	41.2	<12.70	...	...	1.21	<29.47	
78	Hz883/T70b	...	...	40.9	<12.67	...	...	1.21	<29.47	
79	Hz890/A121	...	...	30.0	<4.85	...	...	1.21	<29.06	
80	Hz915/T71b/MT67	-3.7	-2.8	34.3	17.83	11.63	2.32 ± 0.36	1.42	29.69	4
81	Hz906/T14/MT65	...	...	47.3	<9.53	...	...	1.21	<29.35	
82	Hz923	-29.1	23.33	34.6	17.83	11.63	2.32 ± 0.36	1.42	29.69	4
83	Hz916	...	...	44.2	<8.39	...	...	1.21	<29.29	
84	Hz930/VM2	2.0	-6.5	12.4	8.09	7.05	1.33 ± 0.36	1.19	29.27	
85	Hz948	...	...	46.9	<7.17	...	...	1.21	<29.23	
86	Hz956	2.2	-2.3	18.9	31.00	12.61	1.60 ± 0.23	1.26	29.88	
87	Hz975	7.1	-6.6	25.7	10.25	7.47	0.97 ± 0.25	1.13	29.35	
88	Hz980	0.6	-2.9	7.2	29.80	18.64	1.30± 0.13	1.19	29.84	
89	Hz996	...	...	40.7	<7.27	...	...	1.21	<29.23	
90	VM6/A2/A76/T46	5.9	-6.0	16.5	4.01	3.84	1.67 ± 0.80	1.27	28.99	
91	Hz1028	...	...	21.9	<8.89	...	...	1.21	<29.32	
92	Hz1032/VM8	11.9	4.1	32.4	65.19	19.83	1.08 ± 0.10	1.14	30.16	

Table 5: Continued

#	Name	$\Delta R.A.$ ["]	$\Delta Dec.$ ["]	Off-axis [']	CtRt	S/N	HR	$cecf$	$\log(L_x)$	Multiple Counterparts
(1)		(2)	(2)		(3)			(4)	(5)	(6)
93*	Hz1039/A148	-4.9	8.1	19.0	13.62	7.81	0.63 ± 0.18	1.97	29.71	
94*	Hz1061/T48/VM9	3.5	0.9	13.6	10.28	8.04	1.56 ± 0.37	3.48	29.84	
95*	Hz1081	...	...	35.8	6.05	3.78	3.45 ± 1.88	5.49	29.80	
96*	Hz1084	...	...	16.8	<3.17	...	...	1.97	<29.08	
97	Hz1094/K3/T195	3.4	-3.8	5.0	5.61	7.60	1.23 ± 0.33	1.17	29.10	
98*	Hz1103/T151	3.5	5.7	29.4	5.51	3.60	0.59 ± 0.43	1.54	29.21	
99	Hz1100/T143b	3.8	-2.2	26.8	23.00	9.50	1.11 ± 0.21	1.14	29.71	
100	SK465	...	...	49.8	<9.25	...	...	1.21	<29.34	
101	Hz1117	1.3	-6.2	7.1	6.42	7.33	1.61 ± 0.41	1.26	29.19	
102	Hz1110/VM12	...	...	37.4	<6.33	...	...	1.21	<29.17	
103	Hz1122	3.7	-3.1	12.4	16.45	10.69	1.38 ± 0.24	1.20	29.58	
104	Hz1124/VM14	5.2	-1.6	8.1	15.11	11.98	1.17 ± 0.19	1.16	29.53	
105*	Hz1136	-1.5	0.6	24.1	47.86	17.4	0.98 ± 0.11	2.26	30.32	
106	Hz1139	...	...	47.3	<7.26	...	...	1.21	<29.23	
107	VM15	3.4	2.2	5.8	2.18	4.00	1.28 ± 0.61	1.18	28.70	
108	Hz1173/T81/MT70	...	...	42.0	<6.56	...	...	1.21	<29.19	
109	SK459	...	...	49.3	<8.10	...	...	1.21	<29.28	
110	HCG245	...	...	49.9	<8.78	...	...	1.21	<29.31	
111	Hz1200	...	...	39.6	8.26	...	...	1.21	<29.18	
112	MT72/VM16/T15	...	...	23.3	5.79	4.12	1.02 ± 0.53	1.13	29.10	
113	Hz1215	-7.9	3.4	18.9	12.04	7.18	1.94 ± 0.48	1.34	29.49	
114	A40	...	...	39.0	6.97	...	...	1.21	<29.19	
115	Hz1234	...	...	37.4	5.99	3.04	1.64 ± 0.93	1.27	29.17	
116	Hz1275	-6.8	-4.9	24.4	4.68	3.55	2.40 ± 1.30	1.43	29.11	
117	Hz1280/T27b/VM19	0.9	0.8	16.0	11.05	8.36	1.23 ± 0.27	1.17	29.40	
118	Hz1284	...	...	6.9	<1.29	...	...	1.21	<28.48	
119	Hz1286/T16	-7.9	0.9	17.4	7.91	6.24	1.30 ± 0.41	1.18	29.26	
120*	Hz1298	19.4	-16.5	11.8	10.69	11.32	1.24 ± 0.21	2.00	29.62	5
121	HCG253	...	...	24.9	10.13	8.23	...	1.21	29.08	6
122	Hz1305/B358	...	...	40.6	8.88	...	...	1.21	<29.24	
123*	Hz1306/T17	-7.5	1.6	12.2	10.69	11.32	1.24 ± 0.21	2.00	29.62	5
124	Hz1321/T28b	-4.1	-0.9	10.6	9.91	8.51	1.55 ± 0.40	1.24	29.38	
125	Hz1309	...	...	23.2	16.09	12.53	...	1.21	29.28	6
126	Hz1332	-4.1	-1.6	12.5	7.44	6.07	1.14 ± 0.36	1.15	29.22	
127	B363	-4.0	0.9	7.1	5.80	7.29	1.18 ± 0.31	1.16	29.11	
128	Hz1338	-0.4	-2.5	15.2	5.85	5.02	2.25 ± 0.89	1.41	29.20	
129	Hz1348/VM24	...	...	30.3	<4.87	...	...	1.21	<29.06	
130*	Hz1355/T45b	-1.1	-0.9	10.7	18.19	11.76	1.03 ± 0.16	1.76	29.79	
131	Hz1362	...	...	16.1	<3.80	...	...	1.21	<28.95	
132	Hz1375	...	...	15.1	<3.50	...	...	1.21	<28.91	
133	Hz1380	...	...	9.4	<1.87	...	...	1.21	<28.64	
134	HCG266	...	...	12.6	2.94	3.75	1.59 ± 0.79	1.25	28.85	
135	Hz1384	4.8	-13.2	42.2	89.38	22.14	1.44 ± 0.11	1.22	30.32	
136	Hz1392	-1.1	-5.6	8.2	9.73	11.73	1.11 ± 0.18	1.15	29.33	7
137	Hz1397	-8.6	-5.6	8.4	9.73	11.73	1.11 ± 0.18	1.15	29.33	7
138	HCG270	...	...	45.8	<8.63	...	...	1.21	<29.31	

Table 5: Continued

#	Name	$\Delta R.A.$ ["]	$\Delta Dec.$ ["]	Off-axis [']	CtRt	S/N	HR	$cecf$	$\log(L_x)$	Multiple Counterparts
(1)		(2)	(2)		(3)			(4)	(5)	(6)
139	Hz1425	...	...	15.9	<2.21	...	...	1.21	<28.72	
140	SK417	...	...	28.6	<4.00	...	...	1.21	<28.97	
141	Hz1432	...	...	15.5	<3.12	...	...	1.21	<28.86	
142	Hz1431	...	...	25.2	<4.53	...	...	1.21	<29.03	
143	HCG273	107.5	-10.3	29.9	6.47	5.63	2.31 ± 0.77	1.42	29.25	8
144	Hz1454/T57b	...	...	48.3	<10.86	...	...	1.21	<29.41	
145	MT78/T105	-2.8	1.8	16.2	9.29	7.10	2.85 ± 0.78	1.50	29.43	
146	Hz1512	-6.8	-10.0	28.3	5.92	4.04	2.58 ± 1.26	1.46	29.22	
147	Hz1516/T64b/MT80	-2.5	11.6	27.0	15.14	6.86	1.48 ± 0.39	1.23	29.56	
148	Hz1514	-38.2	7.3	30.4	6.47	5.63	2.31 ± 0.77	1.42	29.25	8
149	Hz1532/B270	-8.1	-3.9	15.5	18.86	9.92	1.27 ± 0.23	1.18	29.63	
150	Hz1531/T19/VM35	-2.0	-1.9	13.0	17.53	11.35	1.34 ± 0.22	1.19	29.61	
151	ALR513	2.3	21.3	16.0	4.23	4.32	2.20 ± 1.01	1.40	29.06	
152	Hz1593	...	...	43.1	<5.95	...	...	1.21	<29.14	
153	HCG295	-3.0	-2.3	39.1	2.03	3.15	0.64 ± 0.47	1.16	28.66	9
154	A60/B240	-3.0	-2.3	39.1	2.03	3.15	0.64 ± 0.47	1.16	28.66	9
155	ALR929	-16.6	-6.3	39.2	2.03	3.15	0.64 ± 0.47	1.16	28.66	9
156	Hz1613	0.6	-6.0	14.9	12.36	8.27	1.66 ± 0.37	1.27	29.48	
157	HCG302	...	...	38.1	<5.51	...	...	1.21	<29.11	
158	ALR928	...	...	40.9	<6.41	...	...	1.21	<29.18	
159	Hz1695/VM38	...	...	20.1	<6.08	...	...	1.21	<29.15	
160	SK384	...	...	41.8	<6.61	...	...	1.21	<29.19	
161	Hz1726	6.9	0.9	23.2	12.11	7.14	1.80 ± 0.47	1.31	29.49	
162	Hz1756	...	...	30.2	<5.18	...	...	1.21	<29.08	
163	Hz1762	2.3	-8.9	31.9	18.19	6.80	1.45 ± 0.38	1.22	29.63	
164	HCG315	7.3	3.1	25.3	8.09	7.62	1.22 ± 0.29	1.17	29.26	10
165	Hz1785/T84/VM41	...	...	41.6	<7.87	...	...	1.21	<29.27	
166	Hz1797	-39.3	-12.7	25.7	8.09	7.62	1.22 ± 0.29	1.17	29.26	10
167	Hz1794/VM42	33.1	-20.8	20.4	4.94	4.46	1.66 ± 0.75	1.27	29.08	11
168	Hz1805/VM43	21.1	-24.8	20.5	4.94	4.46	1.66 ± 0.75	1.27	29.08	11
169	Hz1823	...	...	35.7	<5.94	...	...	1.21	<29.14	
170	Hz1827/T51	...	...	22.1	<8.09	...	...	1.21	<29.28	
171	Hz1856	14.9	-9.6	24.1	7.47	4.71	1.87 ± 0.70	1.32	29.28	
172	HCG332	...	...	48.1	<8.57	...	...	1.21	<29.30	
173	Hz1883/T48b	0.5	7.9	42.6	18.17	7.16	0.52 ± 0.17	1.32	29.67	
174	Hz1876	...	...	35.5	<7.12	...	...	1.21	<29.22	
175	VM46/T156	...	...	32.6	<5.77	...	...	1.21	<29.13	
176	Hz1912	23.6	27.5	29.7	7.27	8.13	2.01 ± 0.47	1.36	29.28	12
177	Hz1924	...	...	37.0	9.94	4.88	2.35 ± 0.89	1.43	29.44	
178	HCG337	-53.5	-79.1	31.7	7.27	8.13	2.01 ± 0.47	1.36	29.28	12
179	Hz1993	...	...	46.6	<9.07	...	...	1.21	<29.33	
180	Hz2016/MT95/T72b	...	...	43.0	<7.37	...	...	1.21	<29.24	
181	Hz2027	...	...	35.4	8.06	3.88	1.18 ± 0.50	1.16	29.26	
182	Hz2034/T9b/VM49	-2.5	-24.6	28.1	26.36	11.11	1.14 ± 0.18	1.15	29.77	
183	ALR728	...	...	33.4	<5.90	...	...	1.21	<29.14	
184	Hz2126	...	...	49.5	<9.17	...	...	1.21	<29.33	

Table 5: Continued

#	Name	$\Delta R.A.$ ["]	$\Delta Dec.$ ["]	Off-axis [']	CtRt	S/N	HR	*cecf*	$\log(L_x)$	Multiple Counterparts
(1)		(2)	(2)		(3)			(4)	(5)	(6)
185	ALR715	...	...	39.7	<6.80	...	...	1.21	<29.20	
186	HCG354	...	...	32.9	<11.33	...	...	1.21	<29.42	
187	Hz2144/T157	...	...	33.0	<11.33	...	...	1.21	<29.42	
188	Hz2147	-21.9	-13.0	32.3	121.31	27.95	1.29 ± 0.08	1.18	30.44	
189	ALR1381	...	...	33.0	<11.52	...	...	1.21	<29.43	
190	Hz2168	...	...	33.7	<5.69	...	...	1.21	<29.13	
191	Hz2181	-7.0	-2.9	35.6	18.82	6.95	2.02± 0.53	1.36	29.70	
192	Hz2193/T88	...	...	38.7	<12.33	...	...	1.21	<29.46	
193	Hz2195	...	...	32.9	<4.71	...	...	1.21	<29.04	
194	Hz2208/T107/A139	...	...	49.3	<10.13	...	...	1.21	<29.38	
195	Hz2220	...	...	45.2	<8.52	...	...	1.21	<29.30	
196	HCG362	...	...	35.3	6.04	...	...	1.21	<29.15	
197	Hz2263	...	...	45.4	<9.21	...	...	1.21	<29.33	
198	HCG363	...	...	38.1	<5.75	...	...	1.21	<29.13	
199	Hz2284/VM57	...	...	35.8	<5.78	...	...	1.21	<29.13	
200	Hz2289	...	...	41.7	<7.86	...	...	1.21	<29.27	
201	Hz2311/VM59	...	...	38.4	<6.48	...	...	1.21	<29.18	
202	Hz2345	...	...	48.8	<9.13	...	...	1.21	<29.33	
203	Hz2341	...	...	38.2	<6.91	...	...	1.21	<29.21	
204	Hz2368/K23	...	...	46.6	<9.15	...	...	1.21	<29.33	
205	Hz2366/VM61	...	...	45.2	57.73	14.18	2.67± 0.36	1.47	<30.22	
206	Hz2425	...	...	41.7	<6.98	...	...	1.21	<29.21	
207	Hz2462/VM64	...	...	43.3	<7.80	...	...	1.21	<29.26	
208	Hz2500	-7.4	-7.8	43.4	34.79	24.64	1.23± 0.09	1.17	29.90	13
209	Hz2503	-14.9	-8.7	43.5	34.79	24.64	1.23± 0.09	1.17	29.90	13
210	Hz2507	-18.0	-10.7	43.5	34.79	24.64	1.23± 0.09	1.17	29.90	13
211	SK293	...	...	45.0	<7.74	...	...	1.21	<29.26	
212	Hz2548/VM69	...	...	47.0	<7.10	...	...	1.21	<29.22	
213	T28	...	...	46.5	<10.84	...	...	1.21	<29.40	
214*	Hz2602/T93	...	...	47.0	<9.14	...	...	1.88	<29.52	

Notes:
(1) Stars with $E(B-V) > 0.1$ are indicated by an asterisk.
(2) Offset are reported for X-ray sources detected with EXSAS or PROS that do not belong to complexes of overlapping sources.
(3) Count rates CtRt, are in units of 10^{-3} ct s^{-1}.
(4) *cecf* is given in units of 10^{-11} ergs cm^{-2} ct^{-1}.
(5) X-ray luminosities are in the form $\log_{10}(L_x[\text{ergs s}^{-1}])$ and are computed for an assumed distance of 127 pc. For the stars B203 (# 58) and Hz2366 (# 205) we quote the X-ray luminosities as upper limits since we attribute the emission from detected sources to different counterparts, cf. §3.2.
(6) Increasing numbers in last column indicate sources identified with more than one star or in complexes of overlapping sources. Stars with the same number are identified with the same X-ray source.

FIGURE CAPTIONS

Figure 1: Apparent magnitude distribution of the optical catalog (solid line); this distribution show a larger number of faint members ($m_V > 15$) compared with the analogous distribution of Figure 2 of Paper I, due to the recent deep optical observations in the core of the cluster. The dotted line indicates the distribution of the stars surveyed with the ROSAT PSPC; dashed line is the magnitude distribution for stars falling in the central region of the FOV, where the sensitivity achieves the greatest value.

Figure 2: ROSAT PSPC image (in the 0.2-2.01 keV passband) of the core of the Pleiades Cluster for the total exposure time retained in our analysis. The bottom gray scale ranges linearly between 1 and 6 counts/pixel. Pixel size is 15″. The window support structure is clearly visible.

Figure 3: H-R diagram of Pleiades stars in our survey. X-ray detections are indicated by filled symbols and undetected stars are denoted by empty symbols. (a) For the entire sample of 214 stars; (b) For the 44 stars in the central region of the FOV.

Figure 4: The maximum likelihood integral X-ray luminosity functions for stars in the Pleiades Cluster. The ordinate represents the probability of finding a star with X-ray luminosity greater than or equal to the X-ray luminosity given on the abscissa. The value of the mean of the logarithm of the luminosity is represented by a cross mark, and vertical marks on either side of it give the 95% confidence limits on the mean obtained by bootstrap analysis. The length of the horizontal solid lines connecting the mean and the confidence limits represents the 99% confidence interval on the mean. (a) Stars with $0 < B - V \leq 0.3$ (dA stars; dotted line) and stars with $0.3 < B - V \leq 0.5$ (dF stars; solid line). The mean luminosity of dF stars is displayed above that for dA stars. (b) Stars with $0.5 < B - V \leq 0.8$ (dG stars). The solid line represents the entire sample, while the dashed line represents stars in regions 1 and 2 only. The mean luminosity of the entire sample is displayed above that for the central regions. (c) Stars with $0.8 < B - V \leq 1.45$ (dK stars). The solid line represents the entire sample, while the dashed line represents stars in regions 1 and 2 only. The mean luminosity of the entire sample is displayed above that for the central regions. (d) Stars with $B - V > 1.45$ (dM stars).

Figure 5: Comparison of Count Rates in Segments A and B. The solid line denotes equality of count rates in the two segments, and the two dashed lines delineate variations by a factor of 2. Filled symbols with associate error bars indicate detections in both segments, and open arrows denote upper limits along the axis they are pointing.

Stars with upper limits in both segments are not plotted. Stars which have varied by a factor of 2 or more have been explicitly labeled.

Figure 6: Comparison of X-ray luminosity for the 99 stars that have been detected in the *Einstein* Survey or in the present survey or in both. The solid line denotes equality of X-ray luminosity in the two surveys, and the two short-dashed and long-dashed lines delineate variations by a factor of 2 and of 5, respectively. Filled symbols indicate detections in both surveys, and open arrows denote upper limits along the axis they are pointing.

Figure 7: Scatter plot of L_x versus $v \sin i$. The dotted line represents the Pallavicini et al. (1981) law derived for late type stars in the solar neighborhood. The solid symbols denote stars falling in the central part of field of view where the censoring affect very little the L_x measurements, while directed arrows denote upper limits on the quantity along the directed axis. (a) For the dG stars in our sample. Solid line represent the best fit to the data. Points show a dependence with a large spread on rotation less steep than the Pallavicini et al. relationship (b) For the dK stars in our sample. In this case the fast rotators have X-ray luminosity much lower than the value predicted by the Pallavicini et al. relationship and there is a substantial fraction of slow rotators with X-ray luminosity comparable to those of the fast rotators.

Figure 8: Scatter plot of the residuals of $\log L_x$ around the best fit regression lines for the Pleiades dG stars versus rotational velocity. The scatter is of the same order of magnitude of that shown in Figure 9b for dK stars and cannot be entirely explained in terms of uncertainties in L_x, $v \cdot \sin i$ or of intrinsic variability.

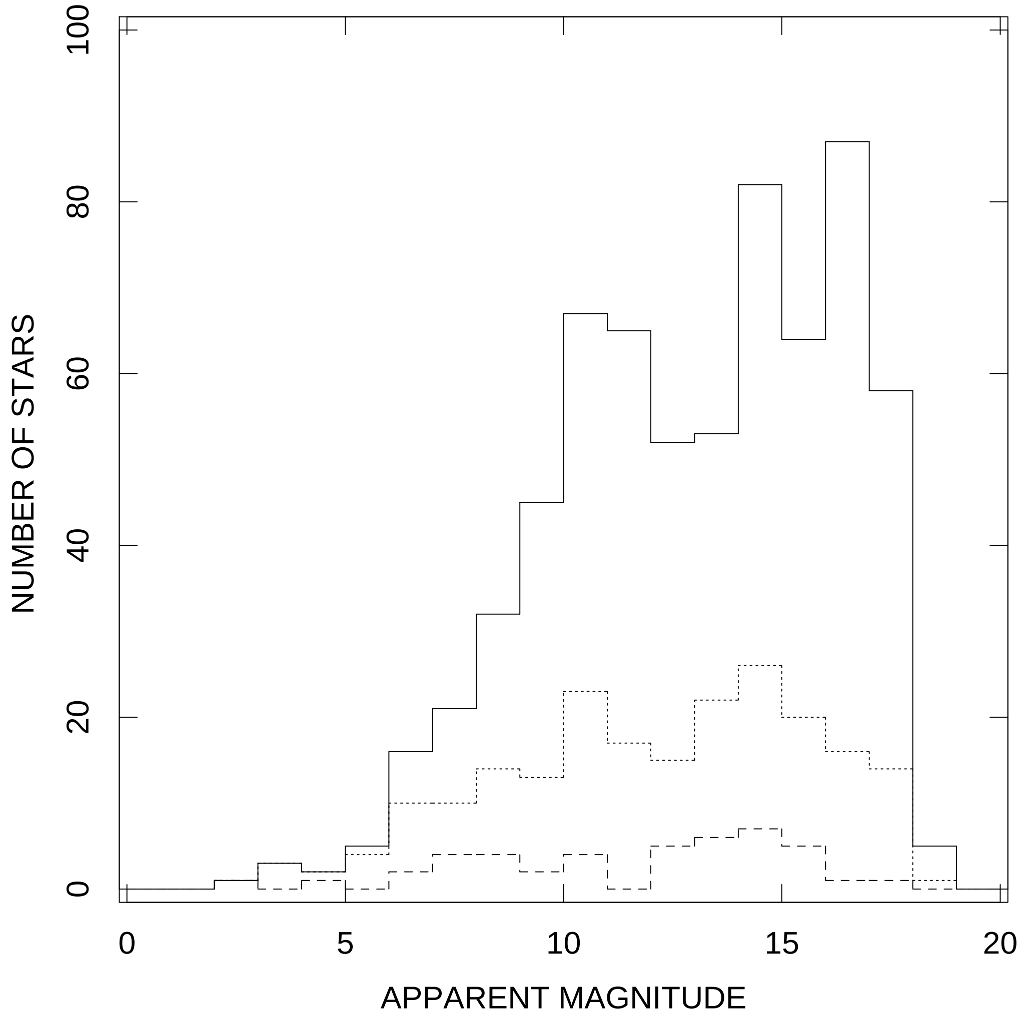
NUMBER OF STARS
0
20
40
60
80
100
0
5
10
15
20
APPARENT MAGNITUDE

Figure 1:

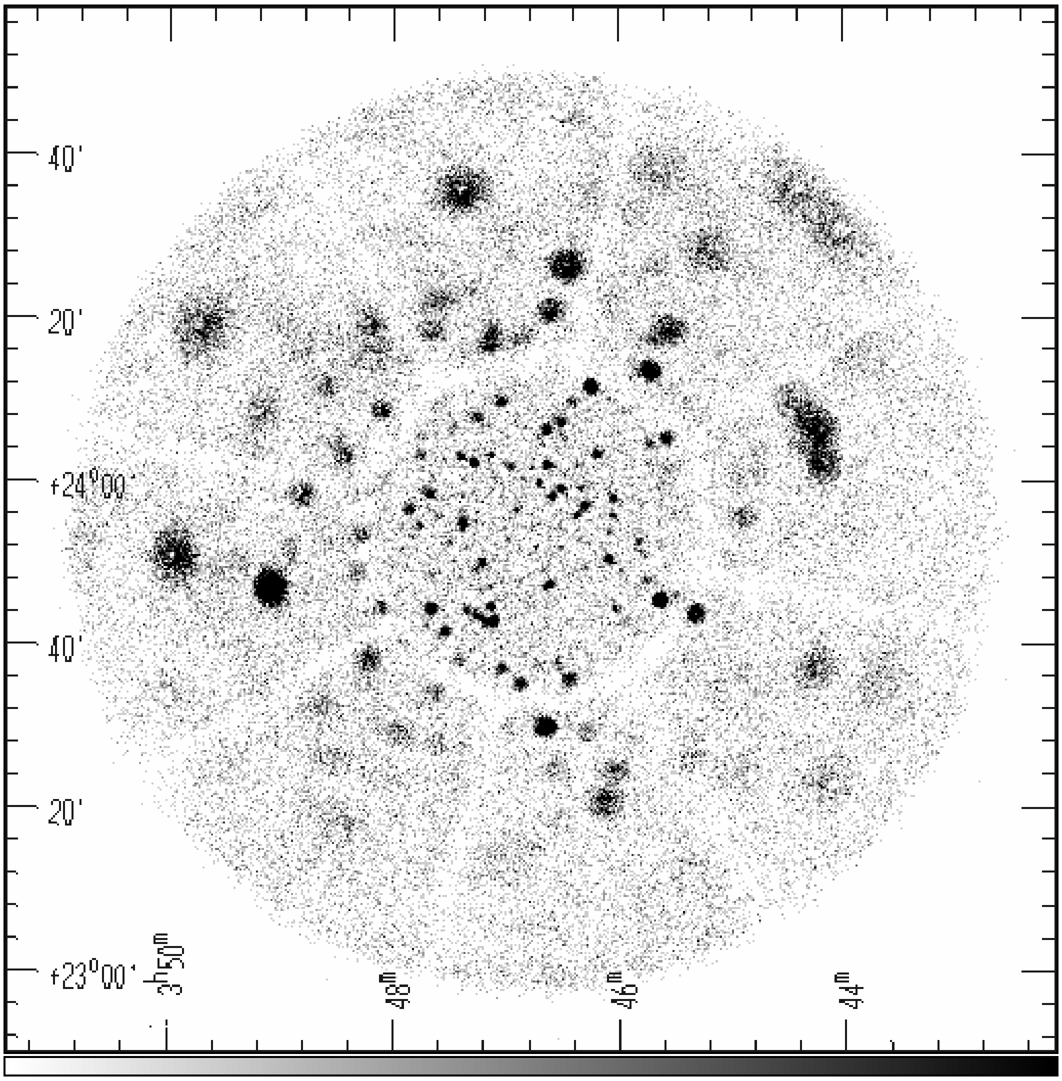

Figure 2:

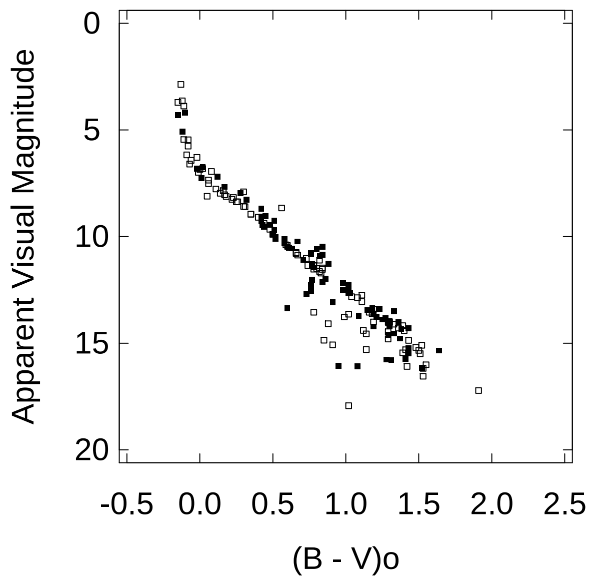

Apparent Visual Magnitude
0
5
10
15
20
-0.5 0.0 0.5 1.0 1.5 2.0 2.5
(B - V)o

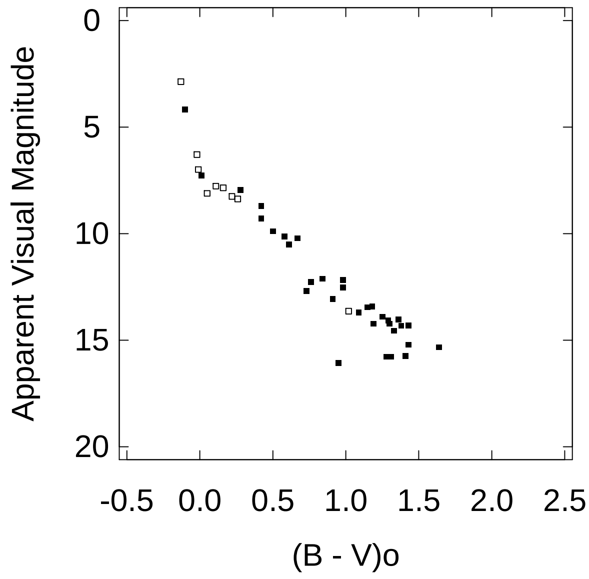

Apparent Visual Magnitude
0
5
10
15
20
-0.5 0.0 0.5 1.0 1.5 2.0 2.5
(B - V)o

Figure 3:

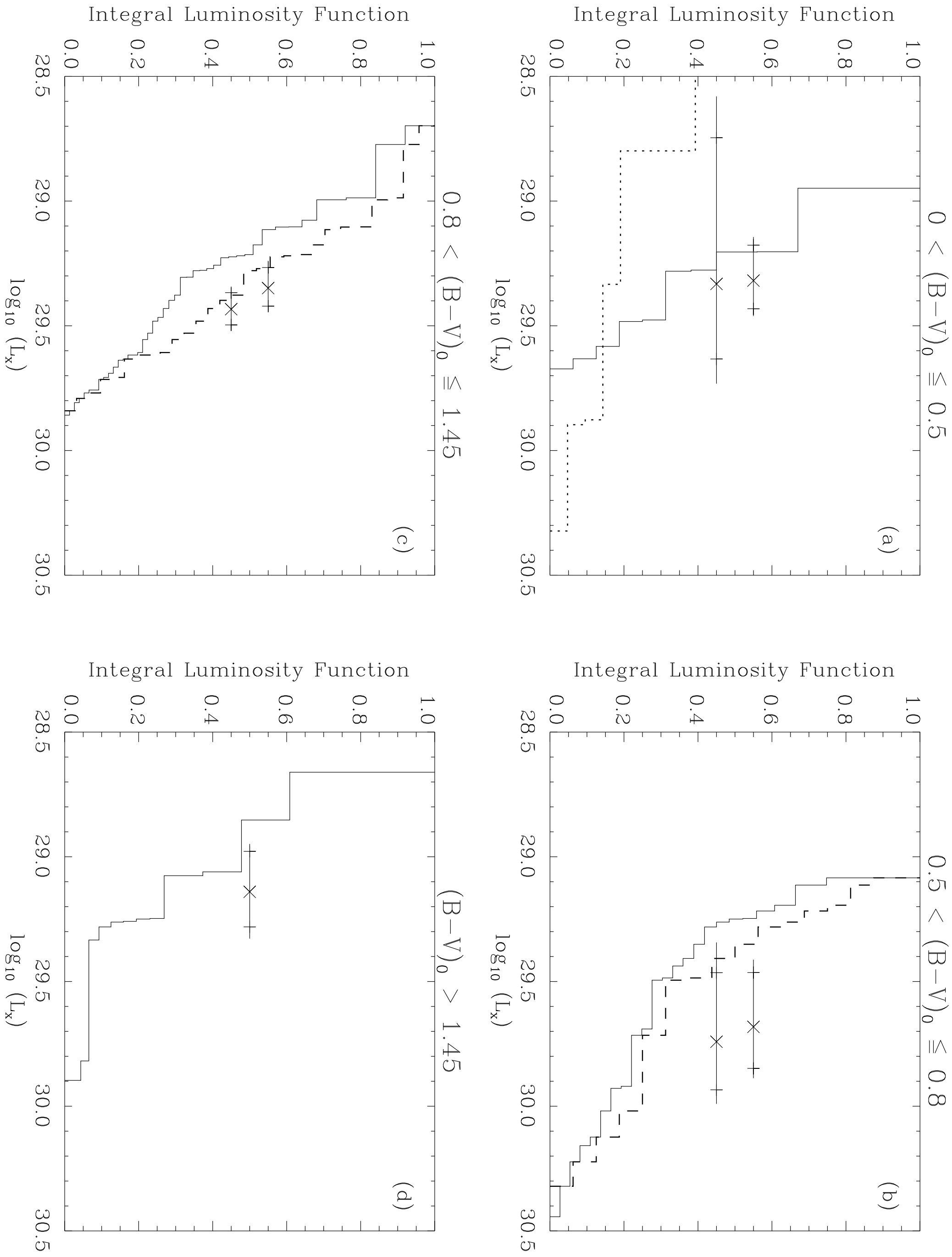

Integral Luminosity Function
$\log_{10}(L_x)$
$0 < (B-V)_0 \le 0.5$
(a)
$0.5 < (B-V)_0 \le 0.8$
(b)
$0.8 < (B-V)_0 \le 1.45$
(c)
$(B-V)_0 > 1.45$
(d)

Figure 4:

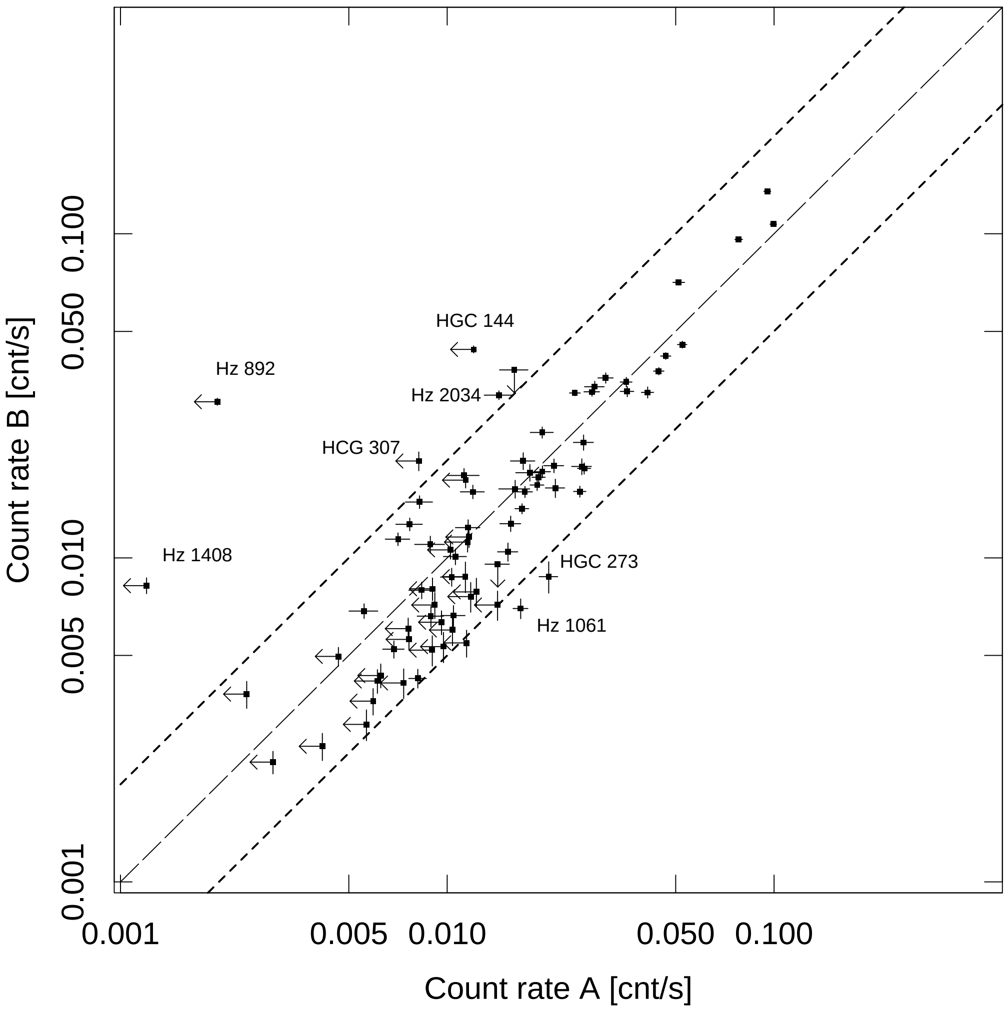

Count rate B [cnt/s]
0.001
0.005
0.010
0.050
0.100
0.001
0.005
0.010
0.050
0.100
Count rate A [cnt/s]
HGC 144
Hz 892
Hz 2034
HCG 307
Hz 1408
HGC 273
Hz 1061

Figure 5:

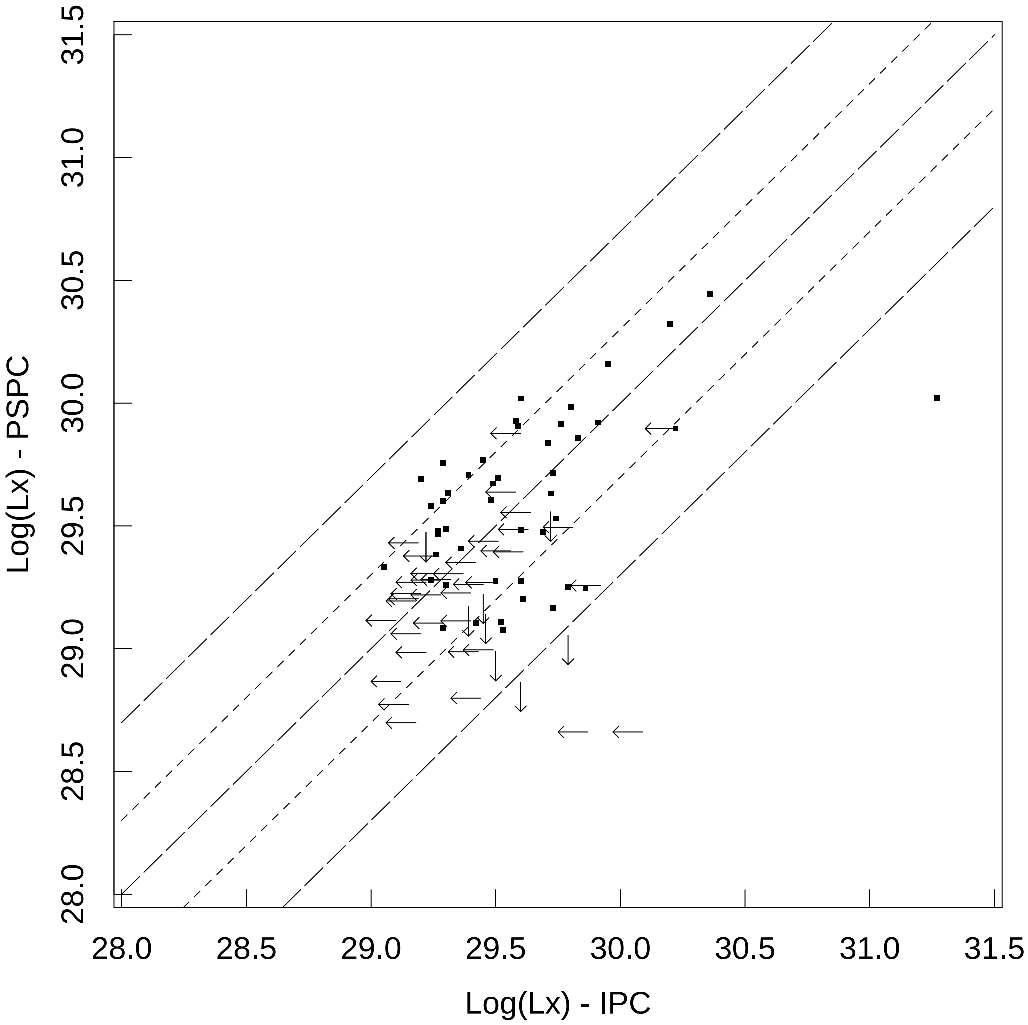

Log(Lx) - PSPC
Log(Lx) - IPC
28.0
28.5
29.0
29.5
30.0
30.5
31.0
31.5
28.0
28.5
29.0
29.5
30.0
30.5
31.0
31.5

Figure 6:

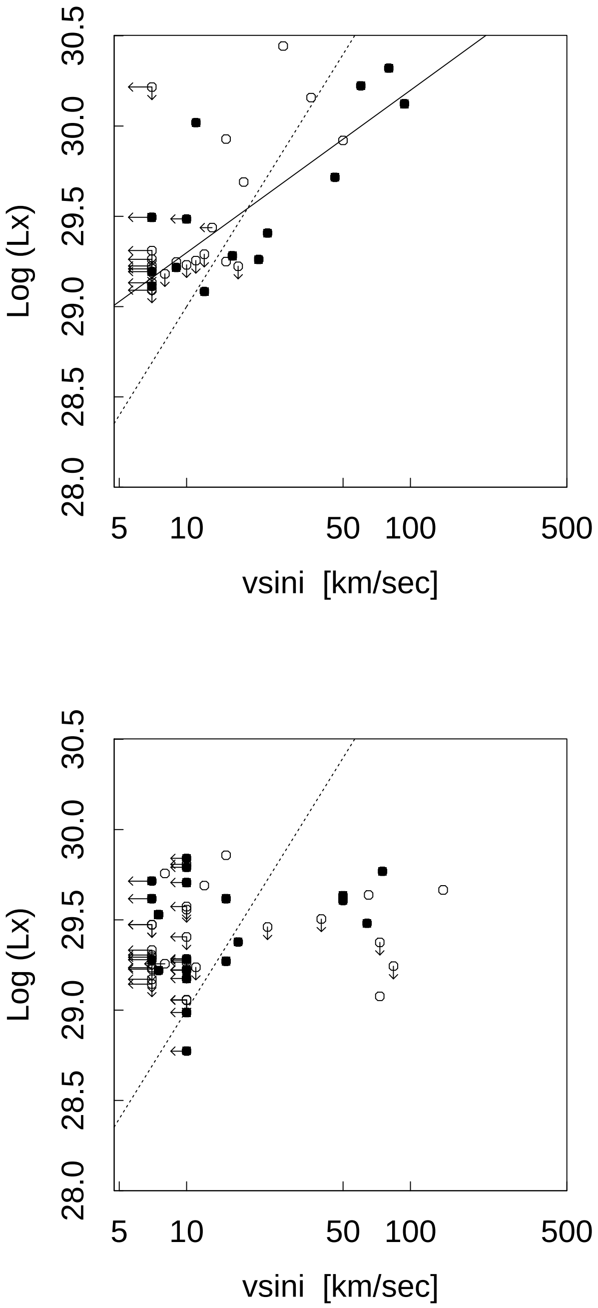

Figure 7:

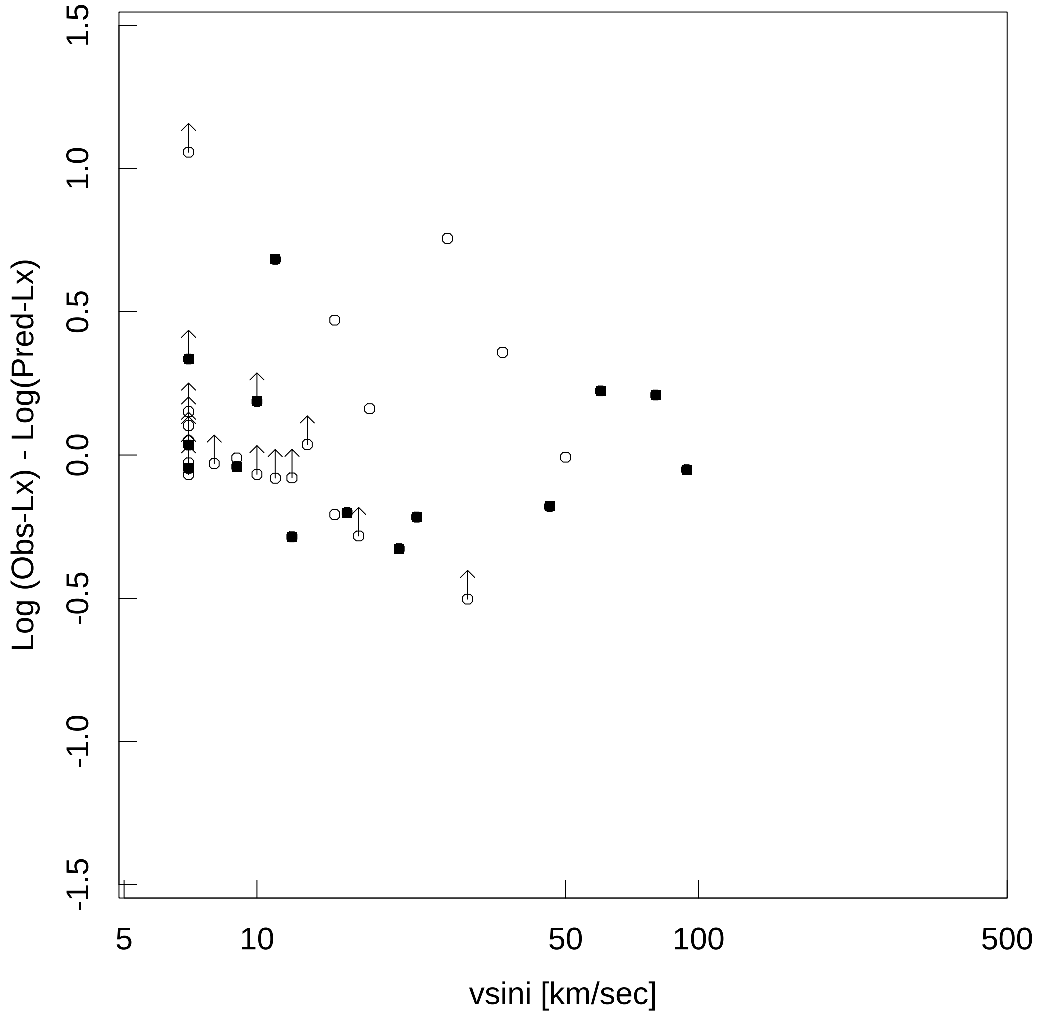
Log (Obs-Lx) - Log(Pred-Lx)
-1.5
-1.0
-0.5
0.0
0.5
1.0
1.5
5
10
50
100
500
vsini [km/sec]

Figure 8: